

Referee 1: Prof. William Collins

We are grateful to Prof. William Collins for his time and energy in providing helpful comments and guidance that have improved the manuscript. In this document, we describe how we have addressed the reviewer's comments. Referee comments are shown in black italics and author responses are shown in blue regular text.

The paper by Yue et al. is a valuable assessment of effects of ozone and aerosol pollution on NPP over China. In particular this is the first time the aerosol contribution has been examined in such detail. The modelled ozone damage is compared against field measurements. This paper should certainly be published in ACP, however some revision is needed as described below.

The authors should make it clearer how much of the impact of ozone and aerosols on NPP is natural and how much anthropogenic. The headline numbers are referred to as due to air pollution, but presumably there would be effects on NPP due to natural ozone. Two extra runs G10NATLO3 and G10NATHO3 would provide the required data for this. The authors assert that since the NPP effect is small below 40 ppb the no ozone and natural ozone simulations are equivalent, but the authors need to demonstrate this with these two extra runs.

→ We performed two extra runs, G10NATLO3_OFF and G10NATHO3_OFF, which consider offline vegetation damages due to O₃ from natural emissions alone. We added a new Figure S7 to compare the GPP reductions caused by O₃ with and without anthropogenic emissions. It shows that O₃ from natural sources has trivial impacts on GPP.

In the Methods section, we revised the text to introduce the two additional experiments: “To compare the differences between online and offline O₃ damage, we perform four additional simulations which do not account for the feedbacks of O₃-induced changes in biometeorology, plant growth, and ecosystem physiology. Two simulations, G10ALLHO3_OFF and G10ALLLO3_OFF, include both natural and anthropogenic emissions. The other two, G10NATHO3_OFF and G10NATLO3_OFF, include natural emissions alone.” (Lines 253-259)

In the Results section, we describe the findings from the extra runs: “Sensitivity simulations with zero anthropogenic emissions show almost no O₃ damage (Fig. S7), because the [O₃] exposure from natural sources alone is usually lower than the threshold level of 40 ppbv below which the damage for most PFTs is limited (Fig. 5).” (Lines 402-405)

When analysing the meteorological changes the authors only show the impacts over China. In their global model set up the aerosols will change globally and affect global circulation (even with fixed SST). The authors should therefore show global maps corresponding to figures 7 and S8 in the supplement. One feature of perturbing aerosols in fixed-SST simulations is that there are large changes in the land-sea temperature

contrast and hence artificial changes in circulation patterns. The resulting meteorological changes over China will therefore be a combination of locally driven effects (such as change in radiation and hence evaporation) and regional-globally driven effects (such as changes in rainfall and hence soil water). This seems to be particularly apparent in the AIE simulations where the patterns of changes in precipitation and soil water bear no relation to the changes in aerosol. The soil moisture changes dominate the aerosol impacts on NPP and I am not convinced these can be attributed to the aerosol changes. The changes in PAR and surface temperature can be much more readily linked physically to the changes in aerosol, therefore the authors should exclude the soil moisture changes from their analysis in table 2.

We do agree that the aerosol-induced changes in meteorology over China are a combination of local and remote effects, but we assert that the changes (local and remote) are all ultimately attributed to the aerosol radiative perturbation. For example, the regional soil moisture changes are absolutely caused by the aerosol radiative perturbations, but may be more linked to a regionally-globally driven dynamical mechanism rather than the reduction in local downward shortwave. The main goal of this study is to investigate the terrestrial biospheric response to air pollution in China. Diagnosing long range dynamical mechanisms is out of scope of this study, especially because the aerosol impacts are so much smaller than the ozone impacts, this specific study will not gain from an explicit description of the multi-scale dynamical mechanisms that drive the regional meteorological changes. Furthermore, the paper is already quite long with 10 figures and supporting information, and global maps obscure and make it difficult for readers to see the regional signals in China. Therefore, we decide not to add further figures of global maps corresponding to figures 7 and S9 in the supplement. In Section 4.1, we already include a comparison of the simulated aerosol impacts on meteorology and surface climate against existing published estimates and a discussion of their realism and uncertainties. Similarly, we select to retain the soil moisture results in Table 3 (original Table 2). Soil moisture dominates the NPP response in only 2 out of 6 scenarios/cases. Even if the soil wetness changes occur in part through more long range dynamical mechanisms triggered by the aerosol radiative perturbations, it is important to highlight the biospheric sensitivity to changes in this driver, oftentimes ignored/neglected in aerosol-carbon-climate studies. For example, precipitation controls GPP in more than 40% of vegetated land (Beer et al., Science, 2010).

Following Prof. Collin's suggestions, we make several modifications.

We add: "The resulting meteorological changes over China are a combination of locally driven effects (such as changes in radiation and hence temperature) and regional-globally driven effects (such as changes in rainfall and hence soil water)." (Lines 431-434).

We clarify: "Aerosol-induced impacts on precipitation and soil moisture are not statistically significant over the regionally averaged domain (Tables S5 and S6). However, for the 2010 and 2030 CLE cases with AIE, 2 out of 6 scenarios, the aerosol-induced impact on soil moisture dominates the total NPP response (Table 3)." (Lines 626-629)

We emphasize: “our estimate of NPP response to aerosol effects, with or without AIE, is secondary in magnitude compared to the O₃ vegetation damage.” (Lines 633-634)

More explanation of table 2 is needed. What simulations are compared against what to derive the answers? How are the uncertainties derived? – presumably they are interannual variability, but different sets of annually-varying data are used for the online and offline calculations.

→ We added more descriptions in the footnote of Table 3 (original Table 2) to explain how we derive those numbers from different simulations. We clarified in the section 2.4.1 about the uncertainties: “The full list of simulations in Table 2 offers assessment of uncertainties due to interannual climate variability, emission inventories (CLE or MTRF), O₃ damage sensitivities (low to high), and aerosol climatic effects (direct and indirect). Uncertainties calculated based on the interannual climate variability in the model are indicated using the format ‘mean ± one standard deviation’. Other sources of uncertainty are explicitly stated.” (Lines 276-281).

The interannual climate variability from online and offline simulations are calculated using different time periods. We clarified in the section 2.4.3 as follows: “Uncertainties due to interannual climate variability in the model are calculated using different time periods for the online (15 years, Table 2) and offline (10 years, Table S3) runs.” (Lines 311-313).

Specific points

Page 2, lines 47-53: Uncertainties (including the range between high and low sensitivity) need to be included here.

→ We included uncertainties due to O₃ sensitivity: “In the present day, O₃ reduces annual NPP by 0.6 Pg C (14%) with a range from 0.4 Pg C (low O₃ sensitivity) to 0.8 Pg C (high O₃ sensitivity). In contrast, aerosol direct effects increase NPP by 0.2 Pg C (5%) through the combination of diffuse radiation fertilization, reduced canopy temperatures, and reduced evaporation leading to higher soil moisture. Consequently, the net effects of O₃ and aerosols decrease NPP by 0.4 Pg C (9%) with a range from 0.2 Pg C (low O₃ sensitivity) to 0.6 Pg C (high O₃ sensitivity). However, precipitation inhibition from combined aerosol direct and indirect effects reduces annual NPP by 0.2 Pg C (4%), leading to a net air pollution suppression of 0.8 Pg C (16%) with a range from 0.6 Pg C (low O₃ sensitivity) to 1.0 Pg C (high O₃ sensitivity).” (Lines 47-56)

Page 2, line 55: suggest to replace “will not alleviate” with “will be further increased”.

→ Corrected as suggested.

Page 4, line 93: “not been properly validated” – The authors need to be more explicit about exactly what deficiencies the previous studies had.

→ We clarified the sentence as follows: “Previous regional modeling ... does not always take advantage of valuable observations to calibrate GPP-O₃ sensitivity coefficients for the China domain and typically the derived results have not been properly validated.” (Lines 94-97)

Page 7, line 186: The authors should clarify that they are referring to 2010 emissions.

→ We clarified as follows: “Inter-comparison of present-day (the year 2010) emissions (Fig. S2) shows ...” (Lines 190-191)

Page 7, line 201: How much does biomass burning contribute to the emissions? Are they considered natural (in G10NATxxx)?

→ We clarified as follows: “Biomass burning emissions, adopted from the IPCC RCP8.5 scenario (van Vuuren et al., 2011), are considered as anthropogenic sources because most fire activities in China are due to human-managed prescribed burning. Compared with the GAINS inventory, present-day biomass burning is equivalent to ≤1% of the emissions for NO_x, SO₂, and NH₃, 1.6% for BC, 3.0% for CO, and 9.6% for OC.” (Lines 213-217)

Page 7, lines 205-210: The authors need to describe how the changes in natural emissions are determined.

→ We add a detailed description of the climate-sensitive natural emission sources:

“The model represents climate-sensitive natural precursor emissions of lightning NO_x, soil NO_x and biogenic volatile organic compounds (BVOCs) (Unger and Yue, 2014). Future 2030 changes in these natural emissions are small compared to the anthropogenic emission changes. Interactive lightning NO_x emissions are calculated based on the climate model’s moist convection scheme that is used to derive the total lightning and the cloud-to-ground lightning frequencies (Price et al., 1997; Pickering et al., 1998; Shindell et al., 2013). Annual average lightning NO_x emissions over China increase by 4% between 2010 and 2030. Interactive biogenic soil NO_x emission is parameterized as a function of PFT-type, soil temperature, precipitation (including pulsing events), fertilizer loss, LAI, NO_x dry deposition rate, and canopy wind speed (Yienger and Levy, 1995). Annual average biogenic soil NO_x emissions increase by only 1% over China between 2010 and 2030. Leaf isoprene emissions are simulated using a biochemical model that depends on the electron transport-limited photosynthetic rate, intercellular CO₂, canopy temperature, and atmospheric CO₂ (Unger et al., 2013). Leaf monoterpene emissions depend on canopy temperature and atmospheric CO₂ (Unger and Yue, 2014). Annual average isoprene emission in China increases by 5% (0.39 TgC/yr) between 2010 and 2030 in response to enhanced GPP and temperature that offset the effects of CO₂-inhibition. Monoterpene emissions decrease by 5% (-0.25 Tg C) between 2010 and 2030 because CO₂-inhibition outweighs the effects of increased warming.” (Lines 220-238).

Page 8, line 217. I suggest including the table of simulations in the main text rather than the supplement.

→ We have moved Table S2 into the main text as suggested (now Table 2).

Page 8, line 232. The authors should list the changes in WMGHG from 2010 to 2030 (at least CO₂ and methane).

→ We clarified as follows: “Well-mixed GHG concentrations are also adopted from the RCP8.5 scenario, with CO₂ changes from 390 ppm in 2010 to 449 ppm in 2030, and CH₄ changes from 1.779 ppm to 2.132 ppm.” (Lines 264-266)

Page, 9 section 2.4.3. This section isn't clear about how the meteorological changes are applied to the offline model. Are they applied as an average (of the last 15 years) of the table S2 simulations; or are individual years from the table S2 simulations used as input. If the former: why is there any variability in the offline output? If the latter: the last 3 years could be strongly influenced by interannual variability.

→ We add one sentence to explain how the meteorological changes are applied to the offline model: “For these simulations, the month-to-month meteorological perturbations caused by aerosols are applied as scaling factors on the baseline forcing.” (Lines 307-309) We actually run the offline simulations for 15 years, with the last 10 years used for the analyses. The paper has been updated for several versions. In the first version, we ran the offline simulations for only 10 years and did not show the uncertainties in the Table because the time period was short. In the latest version, we have already re-ran all simulations to 15 years and calculated uncertainties for Table 3. However, we had omitted to update the corresponding manuscript text.

Page 10, lines 298-299. The agreement in figure 3 doesn't suggest that the “Evaluations at rural sites better match the observations”. The correlation is no better than for all sites, and by eye only the summer points look to show any correlation at all.

→ We revise the text as follows: “Evaluations at rural sites (Table S4), which represent the major domain of China, show a mean bias of -5% (Fig. 3). The magnitude of such bias is much lower than the value of 42.5% for the comparisons at urban-dominant sites (Fig. 2f).” (Lines 346-348)

Page 12, line 346-348. The online model presumably allows the g_s changes to feed back on the ozone concentrations, which should increase them. Therefore it might be expected that the online model would show more ozone damage. The authors should compare the g_s and surface ozone concentration changes between the online and offline models.

→ The online model does allow g_s changes to feed back onto the atmospheric composition. However, our model does not show significant O₃ concentration feedbacks at the current level of vegetation and g_s damage, likely because of multiple offsetting

influences on chemistry. We have now included g_s changes in a revised Figure S6 and described them in the text as follows: “At the same time, the O_3 -induced reductions in stomatal conductance (Fig. S6a) can increase canopy temperature and inhibit plant transpiration, leading to surface warming (Fig. S6b), dry air (Fig. S6c), and rainfall deficit (Fig. S6d).” (Lines 395-398)

Page 12, lines 348-349. Are the authors saying they have carried out a G10NATLO3 simulation, and the NPP change (compared to G10NATNO3) is identically zero everywhere? If so, this needs to be explained more clearly. If not, then the authors need to be clearer about the evidence they have that the zero anthropogenic emissions show no damage. The damage functions in fig 5 don't go exactly to zero at 40 ppb.

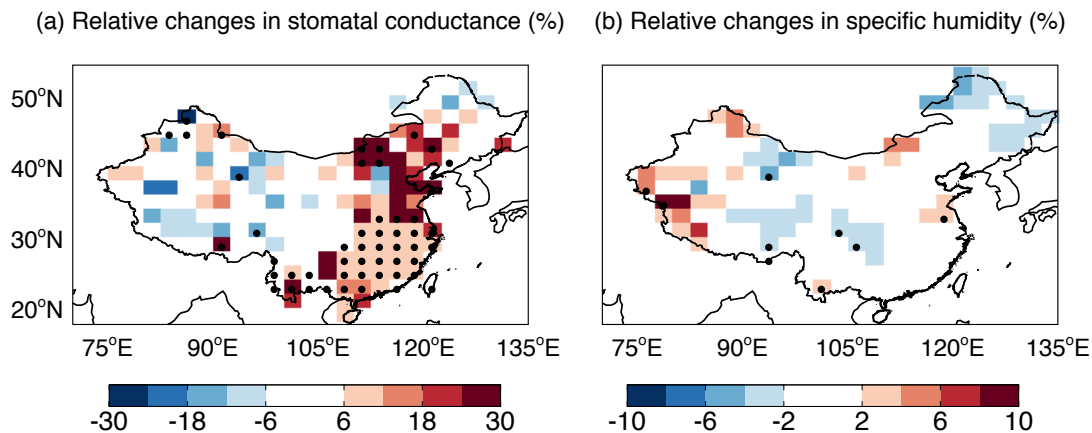
→ We performed two additional sensitivity runs with the climate model ModelE2-YIBs, G10NATLO3_OFF and G10NATHO3_OFF, to examine damages by natural O_3 . We found negligible instead of zero impacts of background O_3 from natural precursor sources in China. We show the results in the new Figure S7. In the main text, we clarified as follows: “Sensitivity simulations with zero anthropogenic emissions show almost no O_3 damage (Fig. S7), because the [O_3] exposure from natural sources alone is usually lower than the threshold level of 40 ppbv below which the damage for most PFTs is limited (Fig. 5).” (Lines 402-405)

Page 12, line 352. The uncertainty here also needs to include the uncertainty in plant sensitivity (i.e. the range from high to low). Technically you should refer to the “central value” between high and low, rather than “average”.

→ We clarified as follows: “Our results indicate that present-day surface O_3 causes strong inhibitions on total NPP in China, ranging from $0.43 \pm 0.12 \text{ Pg C yr}^{-1}$ with low sensitivity to $0.76 \pm 0.15 \text{ Pg C yr}^{-1}$ with high sensitivity (Table 3). The central value of NPP reduction by O_3 is $0.59 \pm 0.11 \text{ Pg C yr}^{-1}$, assuming no direct impacts of O_3 on plant respiration.” (Lines 405-409)

Page 12, line 362. Have the authors checked whether the absolute relative humidity is affected, i.e. whether the relative humidity change is purely due to the decreased temperature.

→ We plotted changes in stomatal conductance and specific humidity (the figure below). It shows that specific humidity changes little. As a result, most of the changes in RH are driven by lower saturation vapor pressure. In the text, we clarified as follows: “Reduced insolation decreases summer surface temperature by 0.63°C in the East, inhibiting evaporation but increasing relative humidity (RH) due to the lower saturation vapor pressure (Table S5). These feedbacks combine to stimulate photosynthesis (Fig. 8a), which, in turn, strengthens plant transpiration (not shown).” (Lines 417-421).



Page 12, lines 363-364. There are a lot of statements presented here without any evidence. The authors have not shown strengthened plant transpiration and have not demonstrated that any increase in RH is due to this (rather than simply decreased temperatures or increased horizontal moisture transport). Similarly the authors have not shown diagnostics demonstrating a direct causal chain between transpiration and precipitation or cloud cover. Both of these could instead be due to changes in circulation patterns.

→ We agree that the original statements were rather terse. As shown above, the increase in transpiration (left panel of the above figure) does not increase specific humidity (right panel). Advection and convergence may alter the local moisture budget. In the revised text, we clarify as follows: “Atmospheric circulation and moisture convergence are also altered due to the pollution-vegetation-climate interactions, resulting in enhanced precipitation (Fig. 7b) and cloud cover (Fig. 7d).” (Lines 421-423)

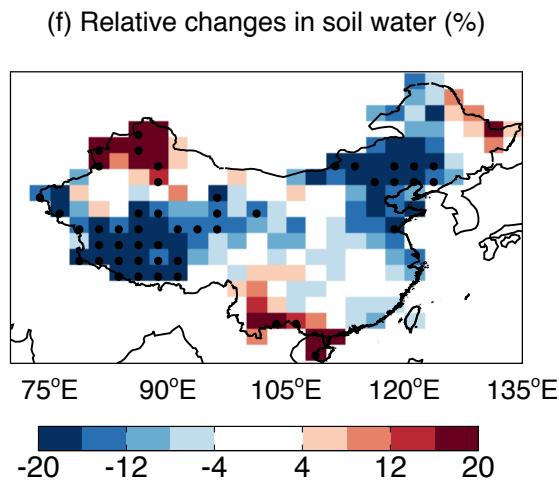
Page 12, lines 367-369. Again no evidence is presented that the decrease in summer precipitation is due to a reduction in the cloud droplet size. Ultimately precipitation is driven by moisture convergence.

→ The precipitation changes are due to a combination of altered cloud microphysics and atmospheric circulation patterns for which we have no way of disentangling. We modify the statement as follows: “Inclusion of AIE results in distinct climatic feedbacks (Fig. S9). Summer precipitation decreases by 0.9 mm day^{-1} (13%), leading to a 3% decline in soil moisture (Table S6).” (Lines 424-426)

Page 13, lines 382-384. This sentence wasn't very clear. Is it referring to changes in heterotrophic respiration? If so, it should be said explicitly.

→ We have removed the sentence about the impact of phenological changes. Quantification of such effects requires additional simulations, which are out of the scope of this study.

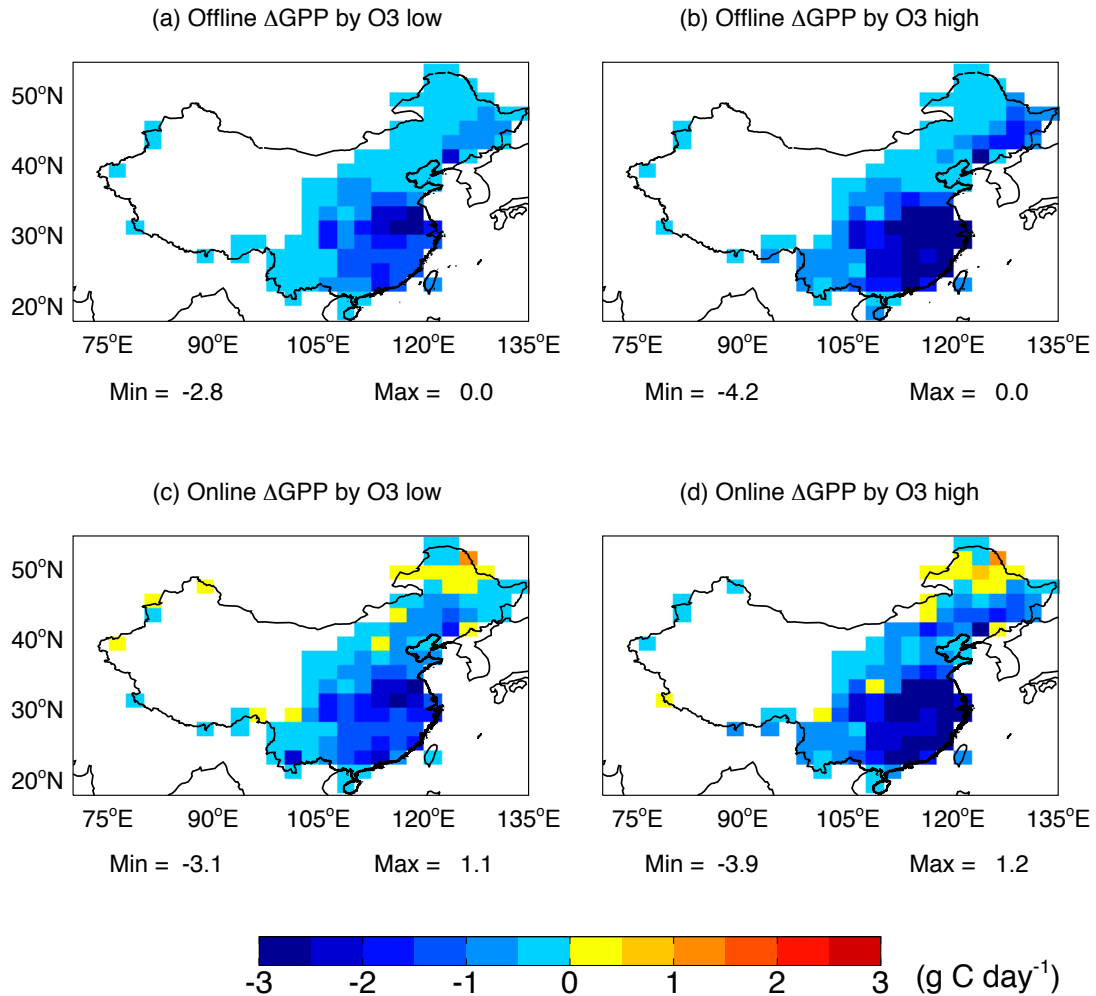
Page 13, line 395. There doesn't seem to be any change in soil water in the North China Plain (fig S8f) in the same region where NPP decreases in fig S9d.



→ The results shown in Fig. S9f (original Fig. S8f) are based on last 15-year simulations (years 6-20). However, results of offline simulations are based on 10-year meteorology (years 6-15). We show the changes in soil moisture for years 6-15 in the above. We can see that the pattern of soil water deficit in the above figure matches NPP changes in Fig. S10d (original Fig. S9d). The changes of soil water in North China Plain are not statistically significant in both the 15-year and 10-year simulations. The lack of significance may cause the inconsistency of NPP changes, i.e., the pattern of Fig. S10d, between the 10-year and 15-year simulations. However, the main conclusion that soil moisture plays the domain role in the NPP responses remains correct because NPP changes by temperature and radiation are far smaller than that by soil moisture. In the text, we added the following statement to remind readers about the discrepancies between online and offline simulations: “Uncertainties due to interannual climate variability in the model are calculated using different time periods for the online (15 years, Table 2) and offline (10 years, Table S3) runs.” (Lines 311-313)

Page 14, line 404. Is the agreement between the offline and online O₃ inhibition true as a geographical pattern as well as the China total?

→ Yes. We show both the online and offline damage below. Although we can see some differences at the individual grid cell level, the spatial patterns are quite similar between the online and offline runs. We do not present the figure in the paper because it is already busy with 10 Figures and supporting information. Instead, we state: “Application of ModelE2-YIBs that allows for these feedbacks gives an O₃-induced damage to annual GPP of 10.7%, a similar level to the damage computed in YIBs offline. The spatial pattern of the online O₃ inhibition also resembles that of offline damages (not shown).” (Lines 399-402)



Page 14, line 406-407. Explain that the range quoted is for no AIE compared to AIE. Uncertainties should also be quoted and include the range between high and low sensitivity.

→ We clarified as follows: “In the year 2010, the combined effects of O₃ and aerosols (Table 3) decrease total NPP in China by 0.39 (without AIE) to 0.80 Pg C yr⁻¹ (with AIE), ...” (Lines 468-470)

We do not add uncertainties of O₃ sensitivity here to avoid redundancy and repetition. Instead, we include those uncertainties in a subsequent sentence: “Independently, O₃ reduces NPP by 0.59 Pg C yr⁻¹, with a large range from 0.43 Pg C yr⁻¹ for low sensitivity to 0.76 Pg C yr⁻¹ for high sensitivity (Table 3).” (Lines 476-478)

Page 14, line 427. What is the change in methane in 2030?

→ In the Methods section, we now describe the changes in CH₄ concentrations: “Well-mixed GHG concentrations are also adopted from the RCP8.5 scenario, with CO₂ changes from 390 ppm in 2010 to 449 ppm in 2030, and CH₄ changes from 1.779 ppm to 2.132 ppm.” (Lines 264-266)

We agree that the increased global [CH₄] also contributes to higher [O₃]. We clarified the sentence as follows: “In contrast, the enhancement of [O₃] results from the increased NO_x emissions, higher level of background CH₄ (~20%), and higher air temperature in the warmer 2030 climate.” (Lines 491-493)

Page 15, lines 434-436. It would be useful to be told the change in g_s between 2010 and 2030.

→ We include the g_s change in the text: “Despite ..., which contributes to g_s inhibition of 4% on the country level, ...”. (Lines 500-501)

Page 15, line 436. Need to include the high-low sensitivity range here.

→ We clarified as follows: “...the future O₃-induced NPP damage in 2030 degrades to 14% or 0.67 Pg C yr⁻¹ (Table 3), with a range from 0.43 Pg C yr⁻¹ (low O₃ sensitivity) to 0.90 Pg C yr⁻¹ (high O₃ sensitivity).” (Lines 501-503)

Page 15, line 441. Need to include the high-low sensitivity range here.

→ We clarified as follows: “The model projects much lower damage to NPP of only 0.12 Pg C yr⁻¹, with a range from 0.06 Pg C yr⁻¹ (low O₃ sensitivity) to 0.20 Pg C yr⁻¹ (high O₃ sensitivity), mainly due to the 40% reduction in [O₃] (Fig. 10c). Including both aerosol direct and indirect effects, O₃ and aerosols together inhibit future NPP by 0.28 Pg C yr⁻¹, ranging from 0.12 Pg C yr⁻¹ with low O₃ sensitivity to 0.43 Pg C yr⁻¹ with high O₃ sensitivity.” (Lines 507-512).

Figure 3. The right hand plot needs a legend to explain the colours.

→ A legend was added as suggested.

Figures 4, 6, 8, 9, 10, S5, S7, S9: The south east China box should be shown in every panel.

→ We prefer to show the box domain only in panel (a) of the figures to be concise and for improved clarity.

Figure 4. The key for blue and black dots should be provided within the graphs.

→ We tried to add the legend for blue and black dots on the scatter plot but found it difficult to place it because of the space limit. It is also inappropriate to place the legend

outside the scatter plot because there are many coloured points in the middle panels (b and e). As a result, we do not make any changes to this Figure.

Figure 5. The key for colours should be provided in the graphs. It would be useful to provide the letter keys within table S1. A different key may be better as there are several authors starting with “Z”.

→ A legend for symbol colours has been added for Figure 5. We added a new column to indicate the abbreviations of references shown in Figure 5. Different authors with the same initials have been differentiated with additional characters. For example, ‘Fo’ represents Foot et al. (1996).

Figure 8. Clarify here and/or in the text that the PAR changes include the DRF.

→ We have added the following sentence in the figure caption: “The NPP responses to PAR include the DRF effects.”

Figure S3. The key for colours should be provided in the graphs.

→ A legend key has been added for Figure S3 as suggested.

Figure S5. The colour scale for percentages should use the red colours for all the positive values, and blue only if there are negative ones, otherwise use the same colours as for the absolute values.

→ We have changed the colour scale for percentages to the same ones as the absolute values in Figure S5.

Referee 2

We are grateful to the reviewer for their time and energy in providing helpful comments and guidance that have improved the manuscript. In this document, we describe how we have addressed the reviewer's comments. Referee comments are shown in black italics and author responses are shown in blue regular text.

This study explores the impact of air pollution on crop production, with a specific focus on China. This is a nice study and in many ways ambitious in scope, though it builds on a series of YIBs model developments described in previous literature. This is a great application of coupling atmospheric chemistry and biosphere modeling and in general I found the paper was well executed. I suggest a little more work to clarify the details behind these results, but after these minor corrections, the paper should be in good shape for publication in ACP.

Specific Comments

1. The paper would benefit from a clearer distinction/discussion of impacts attributed to meteorology feedbacks from PM & O3 forcing vs. aerosol indirect effects. The former are referred to as "direct effects" though they are in fact meteorological feedbacks. In general, it would be helpful if the authors provided a clearer quantification of these specific effects and the model simulations used to assess them.

→ We appreciate that the terminology may be a little challenging in multidisciplinary studies, but we believe that our decisions have made the impacts as clear as possible. We have adopted the use of "direct" and "indirect" as exactly used in the IPCC assessments because these terms are widely used in the aerosol-climate community. The direct and indirect aerosol effects are both associated with meteorological feedbacks. Throughout the manuscript, we emphasize when we are referring to feedbacks and whether they derive from aerosol direct and/or indirect effects.

2. The meteorological & hydrological responses presented primarily in 3.3 should include some standard deviation numbers since multiple years of simulation were run to assess natural variability. Are the changes in soil moisture and precipitation significant?

→ We have separated the original Table S6 into two Tables, with S5 for annual statistics and S6 for summer statistics. Each Table includes the mean changes and one standard deviation (brackets) indicating the uncertainties.

In Section 3.3, we have added following statement to emphasize that the changes in hydrological fields have large uncertainties: "Compared to aerosol-induced perturbations in radiation and temperature, responses in hydrological variables (e.g. precipitation and soil moisture) are usually statistically insignificant on the domain average due to the large relative interannual climate variability (Tables S5 and S6)." (Lines 428-431).

3. *The paper needs a more consistent time-scale. The overall results are presented as annual, however all the figures (except Fig 10) show summertime results only. The authors should either include evaluation for all seasons (or annual means), or present the final results only for summer. As is, the reader cannot judge model skill or response for other seasons.*

→ The reason why our analyses and the Figures focus on the summer is that both GPP/NPP and air pollution (especially O₃) reach maximum at this season. The largest interactions between carbon flux and air pollution are found for this season. It is not a contradiction to show Figures on the summer average and provide annual average impacts because the carbon loss in summer largely dominates the annual total. We found that, for O₃ damages, “about 61% of such inhibition occurs in summer, when both photosynthesis and [O₃] reach maximum of the year.” (Lines 409-410). For the combined O₃ and aerosol effects, “a dominant fraction (60% without AIE and 52% with AIE) of the reduced carbon uptake occurs in summer, when both NPP and [O₃] reach maximum of the year.” (Lines 474-476). We also elect to present and summarize the annual average results to the reader for consistency with regional carbon budget studies. Having the annual average values easily available facilitates comparison with other carbon flux impacts and carbon emissions. For example, we found that: “the combined effects of O₃ and aerosols (Table 3) decrease total NPP in China by 0.39 (without AIE) to 0.80 Pg C yr⁻¹ (with AIE), equivalent to 9-16% of the pollution-free NPP and 16-32% of the total anthropogenic carbon emissions”. (Lines 469-471)

4. *The paper should discuss the potential implications of the high bias in simulated diffuse fraction and potentially in O3 (the evaluation of simulated O3 is mixed).*

→ We added following statements to discuss the implications of biases in diffuse fraction and O₃: “Predicted [O₃] is largely overestimated at urban sites but exhibits reasonable magnitude at rural sites (Figs 2 and 3). Measurements of background [O₃] in China are limited both in space and time, restricting comprehensive validation of [O₃] and the consequent estimate of O₃ damages on the country level.” (Lines 595-598)

“The model overestimates diffuse fraction in China (Fig. 4), likely because of simulated biases in clouds. Previously, we improved the prediction of diffuse fraction in China using observed cloud profiles for the region (Yue and Unger, 2017). Biases in simulated AOD and diffuse fraction introduce uncertainties in the aerosol DRF especially in the affected localized model grid cells. Yet, averaged over the China domain, our estimate of NPP change by aerosol DRF (0.09 Pg C yr⁻¹) is consistent with the previous assessment in Yue and Unger (2017) (0.07 Pg C yr⁻¹).” (Lines 619-625)

Details

1. *Line 71: typo “meteorology, and clouds.”*

→ Corrected as suggested.

2. Line 90: need to define the square brackets in [O₃]

→ We added the following definition: "...O₃ concentrations ([O₃])" (Line 94).

3. Line 93-94: language "less well understood"

→ Corrected as suggested.

4. Line 149-150: not quite true, the CLM includes more PFTs, this should be clarified here.

→ The 8 PFTs used in climate model ModelE2-YIBs are aggregated from a land cover data set with 16 PFTs, which are used by the CLM model. We clarified as follows: "For both global and regional simulations, 8 plant functional types (PFTs) are considered (Fig. S1). This land cover is aggregated from a dataset with 16 PFTs, which are derived using retrievals The same vegetation cover with 16 PFTs is used by the Community Land Model (CLM)" (Lines 150-155).

5. Line 188: this is a large difference in NH₃ emissions, do the authors know why the inventories differ?

→ We clarify as follows: "The discrepancies among different inventories emerge from varied assumptions on the stringency and effectiveness of emission control measures. While the GAINS 2010 ammonia emissions from China are larger than the RCP8.5 and HTAP emissions as shown in Fig. S2, they are close in magnitude to the year 2010 emissions of 13.84 Tg yr⁻¹ estimated by the Regional Emission inventory in ASia (REAS, <http://www.nies.go.jp/REAS/>)." (Lines 193-198)

6. Line 202-203: do these changes in biomass burning emissions seem realistic?

→ The reviewer raises an interesting and provocative question. The future changes in biomass burning in China are small, and that is indeed realistic based on current understanding of fire activity in China today. For example, wildfire activity is limited in China today. We state in the manuscript: "Biomass burning emissions, adopted from the IPCC RCP8.5 scenario (van Vuuren et al., 2011), are considered as anthropogenic sources because most fire activities in China are due to human-managed prescribed burning. Compared with the GAINS inventory, present-day biomass burning is equivalent to <1% of the emissions for NO_x, SO₂, and NH₃, 1.6% for BC, 3.0% for CO, and 9.6% for OC." (Lines 213-217)

7. Lines 205-207: are these natural emissions simulated online or specified? Are there appropriate references that could be cited for this?

→ We add a detailed description of the climate-sensitive natural emission sources:

“The model represents climate-sensitive natural precursor emissions of lightning NO_x, soil NO_x and biogenic volatile organic compounds (BVOCs) (Unger and Yue, 2014). Future 2030 changes in these natural emissions are small compared to the anthropogenic emission changes. Interactive lightning NO_x emissions are calculated based on the climate model’s moist convection scheme that is used to derive the total lightning and the cloud-to-ground lightning frequencies (Price et al., 1997; Pickering et al., 1998; Shindell et al., 2013). Annual average lightning NO_x emissions over China increase by 4% between 2010 and 2030. Interactive biogenic soil NO_x emission is parameterized as a function of PFT-type, soil temperature, precipitation (including pulsing events), fertilizer loss, LAI, NO_x dry deposition rate, and canopy wind speed (Yienger and Levy, 1995). Annual average biogenic soil NO_x emissions increase by only 1% over China between 2010 and 2030. Leaf isoprene emissions are simulated using a biochemical model that depends on the electron transport-limited photosynthetic rate, intercellular CO₂, canopy temperature, and atmospheric CO₂ (Unger et al., 2013). Leaf monoterpene emissions depend on canopy temperature and atmospheric CO₂ (Unger and Yue, 2014). Annual average isoprene emission in China increases by 5% (0.39 TgC/yr) between 2010 and 2030 in response to enhanced GPP and temperature that offset the effects of CO₂-inhibition. Monoterpene emissions decrease by 5% (-0.25 Tg C) between 2010 and 2030 because CO₂-inhibition outweighs the effects of increased warming.” (Lines 220-238).

8. *Lines 208-209: Please explain why isoprene emissions increase and monoterpene emissions decrease (text later indicates that land cover is fixed)*

→ Please see above response to Point (7).

9. *Section 3.1.1 & Figure 1: Please discuss the spatial differences between observed and simulated GPP/NPP.*

→ We add the following information to Section 3.1.1: “For GPP, prediction in the summer overestimates by 6.2% over the southern coast (< 28°N), but underestimates by 23.7% over the North China Plain (NCP, [32-40°N, 110-120°E]). Compared with the MODIS data product, predicted summer NPP is overall overestimated by 20.6% in China (Fig. 1f), with regional biases of 40.0% in the southern coast, 51.2% in the NCP, and 38.7% in the Northeast (> 124°E).” (Lines 327-331)

10. *Line 282: Is R=0.86 a typo? Figure 1 suggests this should be 0.75*

→ The R=0.86 is for the annual GPP as shown in Figure S4. We have indicated both Figure 1 and Figure S4 in the text. (Line 325)

11. *Figure 2 caption: should include years*

→ We added the information of years as follows: “...observations from (b) the satellite retrieval of the MODIS (averaged for 2008-2012), and (e) and (h) measurements from 188 ground-based sites (at the year 2014)” (Lines 959-961)

12. Section 3.1.2 & Figure 2: Please briefly discuss where the model is too high and too low and what species might contribute to these biases. Also quantify the last sentence (line 298-299)

→ We describe the AOD biases as follows: “Predicted AOD also reproduces the observed spatial pattern, but underestimates the high center in NCP by 24.6%.” (Lines 339-340)

In the Discussion Section 4.2, we explain the cause of AOD biases: “Simulated surface PM_{2.5} is reasonable but AOD is underestimated in the North China Plain (Fig. 2), likely because of the biases in aerosol optical parameters. Using a different set of optical parameters, we predicted much higher AOD that is closer to observations with the same aerosol vertical profile and particle compositions (Yue and Unger, 2017).” (Lines 615-619)

We revise the text as follows: “Evaluations at rural sites (Table S4), which represent the major domain of China, show a mean bias of -5% (Fig. 3). The magnitude of such bias is much lower than the value of 42.5% for the comparisons at urban-dominant sites (Fig. 2f).” (Lines 346-348)

13. Line 308: “diffuse fraction agree” – this is incorrect. The simulation appears biased quite high in some regions. Please correct.

→ We corrected the sentence: “Simulated diffuse fraction reproduces observed spatial pattern with high correlation coefficient ($r = 0.74$, $p < 0.01$), though it is on average 25.2% larger than observations (Figs 4d-4f). Such bias is mainly attributed to the overestimation in the North and Northeast. For the southeastern region, where high values of GPP dominate (Fig. 1), predicted diffuse fraction is in general within the 10% difference from the observations.” (Lines 357-362)

14. Section 4.2 should also acknowledge that the response of the hydrological cycle to aerosols is also a major source of uncertainty.

→ We revised the text to acknowledge the uncertainty as follows: “Aerosol-induced impacts on precipitation and soil moisture are not statistically significant over the regionally averaged domain (Tables S5 and S6). However, for the 2010 and 2030 CLE cases with AIE, 2 out of 6 scenarios, the aerosol-induced impact on soil moisture dominates the total NPP response (Table 3).” (Lines 626-629)

1 **Ozone and haze pollution weakens net primary productivity in China**

2
3 Xu Yue¹, Nadine Unger², Kandice Harper³, Xiangao Xia⁴, Hong Liao⁵, Tong Zhu⁶,
4 Jingfeng Xiao⁷, Zhaozhong Feng⁸, and Jing Li⁹

5
6 ¹Climate Change Research Center, Institute of Atmospheric Physics, Chinese Academy of
7 Sciences, Beijing 100029, China

8 ²College of Engineering, Mathematics and Physical Sciences, University of Exeter, Exeter,
9 EX4 4QE, UK

10 ³School of Forestry and Environmental Studies, Yale University, 195 Prospect Street, New
11 Haven, Connecticut 06511, USA

12 ⁴Laboratory for Middle Atmosphere and Global Environment Observation, Institute of
13 Atmospheric Physics, Chinese Academy of Sciences, Beijing 100029, China

14 ⁵School of Environmental Science and Engineering, Nanjing University of Information
15 Science & Technology, Nanjing 210044, China

16 ⁶State Key Laboratory for Environmental Simulation and Pollution Control, College of
17 Environmental Sciences and Engineering, Peking University, Beijing 100871, China.

18 ⁷Earth Systems Research Center, Institute for the Study of Earth, Oceans, and Space,
19 University of New Hampshire, Durham, NH 03824, USA

20 ⁸Research Center for Eco-Environmental Sciences, Chinese Academy of Sciences, Beijing
21 100085, China

22 ⁹Laboratory for Climate and Ocean-Atmosphere Studies, Department of Atmospheric and
23 Oceanic Sciences, School of Physics, Peking University, Beijing 100871, China

24
25
26 *Corresponding author:*

27 Xu Yue

28 Telephone: 86-10-82995369

29 Email: xuyueseas@gmail.com

Deleted: yuexu@mail.iap.ac.cn

30
31
32 *Keywords:* Haze pollution, climate projection, pollution mitigation, ozone damage, diffuse
33 radiative fertilization, aerosol radiative effects, aerosol indirect effects, photosynthesis, net
34 primary productivity

Abstract

37
38
39
40
41
42
43
44
45
46
47
48
49
50
51
52
53
54
55
56
57
58
59
60
61
62
63
64

Atmospheric pollutants have both beneficial and detrimental effects on carbon uptake by land ecosystems. Surface ozone (O_3) damages leaf photosynthesis by oxidizing plant cells, while aerosols promote carbon uptake by increasing diffuse radiation and exert additional influences through concomitant perturbations to meteorology and hydrology. China is currently the world's largest emitter of both carbon dioxide and short-lived air pollutants. The land ecosystems of China are estimated to provide a carbon sink, but it remains unclear whether air pollution acts to inhibit or promote carbon uptake. Here, we employ Earth system modeling and multiple measurement datasets to assess the separate and combined effects of anthropogenic O_3 and aerosol pollution on net primary productivity (NPP) in China. In the present day, O_3 reduces annual NPP by 0.6 Pg C (14%), with a range from 0.4 Pg C (low O_3 sensitivity) to 0.8 Pg C (high O_3 sensitivity). In contrast, aerosol direct effects increase NPP by 0.2 Pg C (5%) through the combination of diffuse radiation fertilization, reduced canopy temperatures, and reduced evaporation leading to higher soil moisture. Consequently, the net effects of O_3 and aerosols decrease NPP by 0.4 Pg C (9%) with a range from 0.2 Pg C (low O_3 sensitivity) to 0.6 Pg C (high O_3 sensitivity). However, precipitation inhibition from combined aerosol direct and indirect effects reduces annual NPP by 0.2 Pg C (4%), leading to a net air pollution suppression of 0.8 Pg C (16%) with a range from 0.6 Pg C (low O_3 sensitivity) to 1.0 Pg C (high O_3 sensitivity). Our results reveal strong dampening effects of air pollution on the land carbon uptake in China today. Following the current legislation emission scenario, this suppression will be further increased by the year 2030, mainly due to a continuing increase in surface O_3 . However, the maximum technically feasible reduction scenario could drastically relieve the current level of NPP damage by 70% in 2030, offering protection of this critical ecosystem service and the mitigation of long-term global warming.

- Deleted: ozone
- Deleted: air pollution
- Deleted: 4 Pg C (9%), resulting from a decrease of 0.
- Deleted: by ozone damage, and an increase of
- Deleted: 2
- Deleted: 5%) by
- Deleted: . The enhancement by aerosols is a
- Deleted: %).
- Deleted: not alleviate
- Deleted: ozone

75 **1 Introduction**

76

77 Surface ozone (O₃) and atmospheric aerosols influence land ecosystem carbon uptake both
78 directly and indirectly through Earth system interactions. O₃ reduces plant photosynthesis
79 directly through stomatal uptake. The level of damage is dependent on both surface ozone
80 concentrations ([O₃]) and the stomatal conductance (g_s), the latter of which is closely
81 related to the photosynthetic rate (Reich and Amundson, 1985; Sitch et al., 2007;
82 Ainsworth et al., 2012). The impact of aerosol pollution on vegetation is less clear.
83 Atmospheric aerosols influence plant photosynthesis through perturbations to radiation,
84 meteorology, and ~~clouds~~. Observations (Cirino et al., 2014; Strada et al., 2015) suggest that
85 an increase in diffuse light partitioning in response to a moderate aerosol loading can
86 improve canopy light use efficiency (LUE) and promote photosynthesis, known as diffuse
87 radiation fertilization (DRF), as long as the total light availability is not compromised
88 (Kanniah et al., 2012). Atmospheric aerosols also reduce leaf temperature (Steiner and
89 Chameides, 2005; Cirino et al., 2014), but the consequence for photosynthesis depends on
90 the relationship between the local environmental temperature and the photosynthetic
91 optimum temperature of approximately 25°C. Aerosol-induced changes in evaporation and
92 precipitation are interconnected but impose opposite effects on photosynthesis; less
93 evaporation preserves soil moisture in the short term but may decrease local rainfall
94 (Spracklen et al., 2012) and lead to drought conditions in the long term. Furthermore,
95 aerosol indirect effects (AIE) on cloud properties can either exacerbate or alleviate the
96 above feedbacks.

97

98 China is currently the world's largest emitter of both carbon dioxide and short-lived air
99 pollutants (<http://gains.iiasa.ac.at/models/>). The land ecosystems of China are estimated to
100 provide a carbon sink (Piao et al., 2009), but it remains unclear how air pollution may affect
101 this sink through the atmospheric influences on regional carbon uptake. O₃ damages to
102 photosynthesis, including those in China, have been quantified in hundreds of
103 measurements (Table S1), but are limited to individual plant species and specific ~~O₃~~
104 ~~concentrations ([O₃])~~. Previous regional modeling of O₃ vegetation damage (e.g., Ren et
105 al., 2011; Tian et al., 2011) does not always take advantage of valuable observations ~~to~~

Deleted: cloud

Deleted: [O₃].

108 [calibrate GPP-O₃ sensitivity coefficients for China domain](#) and typically the derived results
109 have not been properly validated. The aerosol effects on photosynthesis are less [well](#)
110 understood. Most of the limited observation-based studies (Rocha et al., 2004; Cirino et
111 al., 2014; Strada et al., 2015) rely on long-term flux measurements or satellite retrievals,
112 which are unable to unravel impacts of changes in the associated meteorological and
113 hydrological forcings. Modeling studies focus mainly on the aerosol-induced enhancement
114 in diffuse radiation (e.g., Cohan et al., 2002; Gu et al., 2003; Mercado et al., 2009), but
115 ignore other direct and indirect feedbacks such as changes in temperature and precipitation.
116 Finally, no studies have investigated the combined effects of O₃ and aerosols or how the
117 air pollution influences may vary in response to future emission regulations and climate
118 change.

119

120 In this study, we assess the impacts of O₃ and aerosols on land carbon uptake in China
121 using the global Earth system model NASA GISS ModelE2 that embeds the Yale
122 Interactive Terrestrial Biosphere model (YIBs). This framework is known as NASA
123 ModelE2-YIBs and fully couples the land carbon-oxidant-aerosol-climate system (Schmidt
124 et al., 2014; Yue and Unger, 2015). The global-scale model accounts for long-range
125 transport of pollution and large-scale feedbacks in physical climate change. The coupled
126 Earth system simulations apply present-day and future pollution emission inventories from
127 the Greenhouse Gas and Air Pollution Interactions and Synergies (GAINS) integrated
128 assessment model (<http://gains.iiasa.ac.at/models/>). The simulations include process-
129 based, mechanistic photosynthetic responses to physical climate change, O₃ stomatal
130 uptake, carbon dioxide (CO₂) fertilization, and aerosol radiative perturbations, but not
131 aerosol and acid deposition (Table 1). The O₃ and aerosol haze effects on the land carbon
132 cycle fluxes occur predominantly through changes to gross primary productivity (GPP) and
133 net primary productivity (NPP). Therefore, the current study focuses on GPP and NPP
134 impacts and does not address changes in net ecosystem exchange (NEE).

135

136 **2 Methods**

137

138 **2.1 YIBs vegetation model**

139

140 The YIBs model applies the well-established Farquhar and Ball-Berry models (Farquhar
141 et al., 1980; Ball et al., 1987) to calculate leaf photosynthesis and stomatal conductance,
142 and adopts a canopy radiation scheme (Spitters, 1986) to separate diffuse and direct light
143 for sunlit and shaded leaves. The assimilated carbon is dynamically allocated and stored to
144 support leaf development (changes in leaf area index, LAI) and tree growth (changes in
145 height). A process-based soil respiration scheme that considers carbon flows among 12
146 biogeochemical pools is included to simulate carbon exchange for the whole ecosystem
147 (Yue and Unger, 2015). Similar to many terrestrial models (Schaefer et al., 2012), the
148 current version of YIBs does not include a dynamic N cycle. Except for this deficit, the
149 vegetation model can reasonably simulate ecosystem responses to changes in [CO₂],
150 meteorology, phenology, and land cover (Yue et al., 2015). A semi-mechanistic O₃
151 vegetation damage scheme (Sitch et al., 2007) is implemented to quantify responses of
152 photosynthesis and stomatal conductance to O₃ (Yue and Unger, 2014).

153

154 The YIBs model can be used in three different configurations: site-level, global/regional
155 offline, and online within ModelE2-YIBs (Yue and Unger, 2015). The offline version is
156 driven with hourly 1°×1° meteorological forcings from either the NASA Modern Era
157 Retrospective-analysis for Research and Applications (MERRA) (Rienecker et al., 2011)
158 or the interpolated output from ModelE2-YIBs. The online YIBs model is coupled with the
159 climate model NASA ModelE2 (Schmidt et al., 2014), which considers the interplay
160 among meteorology, radiation, atmospheric chemistry, and plant photosynthesis at each
161 time step. For both global and regional simulations, 8 plant functional types (PFTs) are
162 considered (Fig. S1). This land cover is aggregated from a dataset with 16 PFTs, which are
163 derived using retrievals from both the Moderate Resolution Imaging Spectroradiometer
164 (MODIS) (Hansen et al., 2003) and the Advanced Very High Resolution Radiometer
165 (AVHRR) (Defries et al., 2000). The same vegetation cover with 16 PFTs is used by the
166 Community Land Model (CLM) (Oleson et al., 2010).

167

168 Both the online and offline YIBs models have been extensively evaluated with site-level
169 measurements from 145 globally-dispersed flux tower sites, long-term gridded benchmark

Deleted: data set

Deleted: based on

172 products, and multiple satellite retrievals of LAI, tree height, phenology, and carbon fluxes
173 (Yue and Unger, 2015; Yue et al., 2015). Driven with meteorological reanalyses, the offline
174 YIBs vegetation model estimates a global GPP of $122.3 \pm 3.1 \text{ Pg C yr}^{-1}$, NPP of 63.6 ± 1.9
175 Pg C yr^{-1} , and NEE of $-2.4 \pm 0.7 \text{ Pg C yr}^{-1}$ for 1980-2011, consistent with an ensemble of
176 land models (Yue and Unger, 2015). The online simulations with ModelE2-YIBs,
177 including both aerosol effects and O_3 damage, yield a global GPP of $125.8 \pm 3.1 \text{ Pg C yr}^{-1}$,
178 NPP of $63.2 \pm 0.4 \text{ Pg C yr}^{-1}$, and NEE of $-3.0 \pm 0.4 \text{ Pg C yr}^{-1}$ under present day conditions.
179

180 **2.2 NASA ModelE2-YIBs model**

181

182 The NASA ModelE2-YIBs is a fully coupled chemistry-carbon-climate model with
183 horizontal resolution of $2^\circ \times 2.5^\circ$ latitude by longitude and 40 vertical levels extending to
184 0.1 hPa. The model simulates gas-phase chemistry (NO_x , HO_x , O_x , CO, CH_4 , NMVOCs),
185 aerosols (sulfate, nitrate, elemental and organic carbon, dust, sea salt), and their interactions
186 (Schmidt et al., 2014). Modeled oxidants influence the photochemical formation of
187 secondary aerosol species (sulfate, nitrate, secondary organic aerosol). In turn, modeled
188 aerosols affect photolysis rates in the online gas-phase chemistry (Schmidt et al., 2014).
189 Heterogeneous chemistry on dust surfaces is represented (Bauer et al., 2007). The
190 embedded radiation package includes both direct and indirect (Menon and Rotstain, 2006)
191 radiative effects of aerosols and considers absorption by multiple GHGs. Simulated surface
192 solar radiation exhibits the lowest model-to-observation biases compared with the other 20
193 IPCC-class climate models (Wild et al., 2013). Simulated meteorological and hydrological
194 variables have been full validated against observations and reanalysis products (Schmidt
195 et al., 2014).

196

197 **2.3 Emissions**

198

199 We use global annual anthropogenic pollution inventories from the GAINS integrated
200 assessment model (Amann et al., 2011), which compiles historic emissions of air pollutants
201 for each country based on available international emission inventories and national
202 information from individual countries. Inter-comparison [of present-day \(the year 2010\)](#)

203 emissions (Fig. S2) shows that the GAINS V4a inventory has similar emission intensity
204 (within $\pm 10\%$) in China as IPCC RCP8.5 scenario (van Vuuren et al., 2011) for most
205 species, except for ammonia, which is higher by 80% in GAINS. The discrepancies among
206 different inventories emerge from varied assumptions on the stringency and effectiveness
207 of emission control measures. While the GAINS 2010 ammonia emissions from China are
208 larger than the RCP8.5 and HTAP emissions as shown in Fig. S2, they are close in
209 magnitude to the year 2010 emissions of 13.84 Tg yr⁻¹ estimated by the Regional Emission
210 inventory in ASia (REAS, <http://www.nies.go.jp/REAS/>).

211
212 The GAINS inventory also projects medium-term variations of future emissions at five-
213 year intervals to the year 2030. The current legislation emissions (CLE) scenario applies
214 full implementation of national legislation affecting air pollution emissions; for China, this
215 represents the 11th five-year plan, including known failures. By 2030, in the CLE inventory,
216 CO decreases by 18%, SO₂ by 21%, black carbon (BC) by 28%, and organic carbon (OC)
217 by 41%, but NO_x increases by 20%, ammonia by 22%, and non-methane volatile organic
218 compounds (NMVOC) by 6%, relative to the 2010 emission magnitude in China. To
219 account for potential rapid changes in policy and legislation, we apply the maximum
220 technically feasible reduction (MTFR) emission scenario as the lower limit of future air
221 pollution. The MTFR scenario implements all currently available control technologies,
222 disregarding implementation barriers and costs. With this scenario, the 2030 emissions of
223 NO_x decrease by 76%, CO by 79%, SO₂ by 67%, BC by 81%, OC by 89%, ammonia by
224 65%, and NMVOC by 62% in China, indicating large improvement of air quality. Biomass
225 burning emissions, adopted from the IPCC RCP8.5 scenario (van Vuuren et al., 2011), are
226 considered as anthropogenic sources because most fire activities in China are due to
227 human-managed prescribed burning. Compared with the GAINS inventory, present-day
228 biomass burning is equivalent to <1% of the emissions for NO_x, SO₂, and NH₃, 1.6% for
229 BC, 3.0% for CO, and 9.6% for OC. By the year 2030, biomass burning emissions decrease
230 by 1-2% for all pollution species compared with 2010.

231
232 The model represents climate-sensitive natural precursor emissions of lightning NO_x, soil
233 NO_x and biogenic volatile organic compounds (BVOCs) (Unger and Yue, 2014). Future

Deleted: black carbon

Deleted: organic carbon

Deleted: at the year 2030

Deleted: Natural emissions of air pollution show much smaller changes by 2030 compared with anthropogenic emissions. Lightning NO_x emissions increase by ~4% (0.02 Tg N) and soil NO_x emissions increase by ~1% (0.001 Tg N). Emissions of biogenic VOCs, predicted with a photosynthesis-based scheme (Yue et al., 2015), increase by 5% (+0.39 Tg C) for isoprene but decrease by 5% (-0.25 Tg C) for monoterpenes. Changes in natural emissions of SO₂ (volcano and ocean sources) and NH₃ (ocean source) are trivial over China.

247 2030 changes in these natural emissions are small compared to the anthropogenic emission
248 changes. Interactive lightning NO_x emissions are calculated based on the climate model's
249 moist convection scheme that is used to derive the total lightning and the cloud-to-ground
250 lightning frequencies (Price et al., 1997; Pickering et al., 1998; Shindell et al., 2013).
251 Annual average lightning NO_x emissions over China increase by 4% between 2010 and
252 2030. Interactive biogenic soil NO_x emission is parameterized as a function of PFT-type,
253 soil temperature, precipitation (including pulsing events), fertilizer loss, LAI, NO_x dry
254 deposition rate, and canopy wind speed (Yienger and Levy, 1995). Annual average
255 biogenic soil NO_x emissions increase by only 1% over China between 2010 and 2030. Leaf
256 isoprene emissions are simulated using a biochemical model that depends on the electron
257 transport-limited photosynthetic rate, intercellular CO₂, canopy temperature, and
258 atmospheric CO₂ (Unger et al., 2013). Leaf monoterpene emissions depend on canopy
259 temperature and atmospheric CO₂ (Unger and Yue, 2014). Annual average isoprene
260 emission in China increases by 5% (0.39 Tg C yr⁻¹) between 2010 and 2030 in response to
261 enhanced GPP and temperature that offset the effects of CO₂-inhibition. Monoterpene
262 emissions decrease by 5% (-0.25 Tg C) between 2010 and 2030 because CO₂-inhibition
263 outweighs the effects of increased warming.

264

265 **2.4 Simulations**

266

267 **2.4.1 NASA ModelE2-YIBs online**

268 We perform 24 time-slice simulations to explore the interactive impacts of O₃ and aerosols
269 on land carbon uptake (Table 2). All simulations are performed in atmosphere-only
270 configuration. In these experiments, [O₃] and aerosol loading are dynamically predicted,
271 and atmospheric chemistry processes are fully two-way coupled to the meteorology and
272 the land biosphere. Simulations can be divided into two groups, depending on whether AIE
273 are included. In each group, three subgroups are defined with the emission inventories of
274 GAINS 2010, CLE 2030, and MTRF 2030 scenarios. In each subgroup, one baseline
275 experiment is set up with only natural emissions, (denoted with NAT). The other three
276 implement all natural and anthropogenic sources of emissions, (denoted with ALL), but
277 apply different levels of O₃ damage including none, (denoted with NO3), low sensitivity,

Deleted: S2

Deleted: .

Deleted: ,

Deleted: ,

Deleted: ,

283 (LO3), and high sensitivity,(HO3). To compare the differences between online and offline
284 O₃ damage, we perform four additional simulations, which do not account for the feedbacks
285 of O₃-induced changes in biometeorology, plant growth, and ecosystem physiology. Two
286 simulations, G10ALLHO3 OFF and G10ALLLO3 OFF, include both natural and
287 anthropogenic emissions. The other two, G10NATHO3 OFF and G10NATLO3 OFF,
288 include natural emissions alone.

Deleted: .

Deleted: two

Deleted: , G10ALLHO3_OFF and G10ALLLO3_OFF,

289
290 We use prescribed sea surface temperature (SST) and sea ice distributions simulated by
291 ModelE2 under the IPCC RCP8.5 scenario (van Vuuren et al., 2011). For these boundary
292 conditions, we apply the monthly-varying decadal average of 2006-2015 for 2010
293 simulations and that of 2026-2035 for 2030 simulations. Well-mixed GHG concentrations
294 are also adopted from the RCP8.5 scenario, with CO₂ changes from 390 ppm in 2010 to
295 449 ppm in 2030, and CH₄ changes from 1.779 ppm to 2.132 ppm. Land cover change
296 projections for this scenario suggest only minor changes between the years 2010 and 2030;
297 for example, the expansion of 3% for grassland is offset by the losses of 1% for cropland
298 and 4% for tropical rainforest. As a result, we elect to apply the same land cover, which is
299 derived from satellite retrievals, for both present-day and future simulations (Fig. S1). We
300 use present-day equilibrium tree height derived from a 30-year spinup procedure (Yue and
301 Unger, 2015) as the initial condition. All simulations are performed for 20 years, and the
302 last 15 years are used for analyses. For simulations including effects of CO₂ fertilization,
303 climate change, and O₃ damages, GPP and NPP reach new equilibrium within 5 years while
304 those for NEE may require several decades due to the slow responses of the soil carbon
305 pools (Fig. S3). The full list of simulations in Table 2 offers assessment of uncertainties
306 due to interannual climate variability, emission inventories (CLE or MTR), O₃ damage
307 sensitivities (low to high), and aerosol climatic effects (direct and indirect). Uncertainties
308 calculated based on the interannual climate variability in the model are indicated using the
309 format 'mean ± one standard deviation'. Other sources of uncertainty are explicitly stated.

Deleted: .

311 2.4.2 YIBs offline with MERRA meteorology

312 We perform 15 simulations to evaluate the skill of the O₃ damage scheme for vegetation in
313 China (Table S2). Each run is driven with hourly meteorological forcings from NASA

Deleted: S3

319 GMAO MERRA (Rienecker et al., 2011). One baseline simulation is performed without
320 inclusion of any O₃ damage. The others, seven runs in each of two groups, are driven with
321 fixed [O₃] at 20, 40, 60, 80, 100, 120, and 140 ppbv, respectively, using either low or high
322 O₃ sensitivities defined by (Sitch et al., 2007). Thus, [O₃] in these offline runs is fixed
323 without seasonal and diurnal variations to mimic field experiments that usually apply a
324 constant level of [O₃] during the test period. We compare the O₃-affected GPP with the O₃-
325 free GPP from the baseline simulation to derive the damaging percentages to GPP, which
326 are compared with values for different PFTs from an ensemble of published literature
327 results (Table S1). All simulations are performed for 1995-2011, and the last 10 years are
328 used for analyses.

329

330 **2.4.3 YIBs offline with ModelE2-YIBs meteorology**

331 Using the offline YIBs vegetation model driven with ModelE2-YIBs meteorology, we
332 perform 30 simulations to isolate the impacts of aerosol-induced changes in the individual
333 meteorological drivers on carbon uptake (Table S3). Experiments are categorized into two
334 groups, depending on whether the GCM forcings include AIE or not. In each group, three
335 subgroups of simulations are set up with different meteorology for GAINS 2010, CLE
336 2030, and MTRF 2030 scenarios. Within each subgroup, five runs are designed with the
337 different combinations of GCM forcings. One baseline run is forced with meteorology
338 simulated without anthropogenic aerosols. The other four are additionally driven with
339 aerosol-induced perturbations in temperature, PAR, soil moisture, or the combination of
340 the above three variables. For these simulations, the month-to-month meteorological
341 perturbations caused by aerosols are applied as scaling factors on the baseline forcing. The
342 differences of NPP between sensitivity and baseline runs represent contributions of
343 individual or total aerosol effects. Each simulation is performed for 15 years, with the last
344 10 years used for analyses. Uncertainties due to interannual climate variability in the model
345 are calculated using different time periods for the online (15 years, Table 2) and offline (10
346 years, Table S3) runs.

347

348 **3 Results**

349

Deleted: S4

Deleted: 10 years, with the last 3 years used for analyses

Formatted: Font:Times New Roman, Font color:
Auto

352 3.1 Evaluation of ModelE2-YIBs over China

353

354 3.1.1 Land carbon fluxes: GPP and NPP

355 To validate simulated GPP, we use a gridded benchmark product for 2009-2011 upscaled
356 from *in situ* FLUXNET measurements (Jung et al., 2009). For NPP, we use a MODIS
357 satellite-derived product for 2009-2011 (Zhao et al., 2005). Both datasets are interpolated
358 to the same resolution of $2^{\circ} \times 2.5^{\circ}$ as ModelE2-YIBs. Simulated GPP and NPP reproduce
359 the observed spatial patterns with high correlation coefficients ($R=0.46-0.86$, $p < 0.001$)
360 and relatively low model-to-observation biases ($< 20\%$) (Fig. 1 and Fig. S4). High values
361 of the land carbon fluxes are predicted in the East and the Northeast, where forests and
362 croplands dominate (Fig. S1). For GPP, prediction in the summer overestimates by 6.2%
363 over the southern coast ($< 28^{\circ}\text{N}$), but underestimates by 23.7% over the North China Plain
364 (NCP, [$32-40^{\circ}\text{N}$, $110-120^{\circ}\text{E}$]). Compared with the MODIS data product, predicted
365 summer NPP is overall overestimated by 20.6% in China (Fig. 1f), with regional biases of
366 40.0% in the southern coast, 51.2% in the NCP, and 38.7% in the Northeast ($> 124^{\circ}\text{E}$).

367

368 3.1.2 Surface air pollution and AOD

369 For surface concentrations of $\text{PM}_{2.5}$ and O_3 , we use ground measurements available for
370 2014 from 188 sites operated by the Ministry of Environmental Protection of China
371 (<http://www.aqicn.org/>). In addition, we use rural [O_3] from published literature (Table S4)
372 to evaluate the model. For AOD, we use gridded observations of 2008-2012 from MODIS
373 retrievals. The model simulates reasonable magnitude and spatial distribution of surface
374 $\text{PM}_{2.5}$ concentrations (Fig. 2). Predicted AOD also reproduces the observed spatial pattern,
375 but underestimates the high center in NCP by 24.6%. Long-term measurements of [O_3] are
376 very limited in China. Comparisons with the 2014 one-year data from 188 urban sites show
377 that simulated [O_3] reproduces reasonable spatial distribution but overestimates the average
378 concentration by $>40\%$. Such discrepancy is in part attributed to the sampling biases,
379 because urban [O_3] is likely lower than rural [O_3] due to high NO_x emissions (NO_x titration)
380 and aerosol loading (light extinction) in cities. Evaluations at rural sites (Table S4), which
381 represent the major domain of China, show a mean bias of -5% (Fig. 3). The magnitude of

Deleted: ModelE

Deleted: S5

Deleted: AOD and

Deleted: S5) better match the observations that

Formatted: Font:Times

386 such bias is much lower than the value of 42.5% for the comparisons at urban-dominant
387 sites (Fig. 2f).

388

389 **3.1.3 Shortwave radiation**

390 We use ground-based observations of surface shortwave radiation and diffuse fraction from
391 106 pyranometer sites managed by the Climate Data Center, Chinese Meteorological
392 Administration (Xia, 2010). Site selection is based on the availability of continuous
393 monthly measurements during 2008-2012, resulting in 95 sites for the evaluation of total
394 shortwave radiation. For diffuse radiation, we select the 17 sites only that provide
395 continuous measurements during 2008-2012. Simulated surface shortwave radiation agrees
396 well with measurements at 106 sites (Figs 4a-4c). Simulated diffuse fraction reproduces
397 observed spatial pattern with high correlation coefficient ($r = 0.74$, $p < 0.01$), though it is
398 on average 25.2% larger than observations (Figs 4d-4f). Such bias is mainly attributed to
399 the overestimation in the North and Northeast. For the southeastern region, where high
400 values of GPP dominate (Fig. 1), predicted diffuse fraction is in general within the 10%
401 difference from the observations.

402

403 **3.1.4 Ozone vegetation damage function**

404 We adopt the same approach as Yue et al. (2016) by comparing simulated GPP-to-[O₃]
405 responses (Table S2) with observations from multiple published literature (Table S1). We
406 aggregate these measurements into six categories, including evergreen needleleaf forest
407 (ENF), deciduous broadleaf forest (DBF), shrubland, C3 herbs, C4 herbs, and a mixture of
408 all above species. We derive the sensitivity of GPP to varied [O₃] (Fig. 5) using the YIBs
409 offline version. For most PFTs, simulated O₃ damage increases with [O₃] in broad
410 agreement with measurements. Predicted O₃ damage reproduces observations with a
411 correlation coefficient of 0.61 (for all samplings, $n=32$) and in similar magnitudes (-17.7%
412 vs. -20.4%), suggesting that the damage scheme we adopted from Sitch et al. (2007) is
413 ready to use in China. For the same level of [O₃], deciduous trees suffer larger damages
414 than evergreen trees because the former species are usually more sensitive (Sitch et al.,
415 2007) and have higher g_s (therefore higher uptake) (Wittig et al., 2007). Flux-based O₃
416 sensitivity for C4 herbs is only half that of C3 herbs (Sitch et al., 2007), however,

Deleted: and diffuse fraction agree well with measurements at 106 sites, especially over the East where low solar insolation while high diffusion are predicted (Fig. 4).

Deleted: S3

421 concentration-based O₃ damages, both observed and simulated, are larger for C4 plants
422 because of their higher uptake efficiency following high g_s (Yue and Unger, 2014).

423

424 3.2 O₃ effects in China

425

426 We focus our study domain in eastern China (21°-38°N, 102°-122°E, including the North
427 China Plain, the Yangtze River Delta, and part of the Sichuan Basin), a region that suffers
428 from high levels of O₃ and aerosols from anthropogenic pollution sources (>75%
429 contribution; Fig. S5). We estimate that surface O₃ decreases annual GPP in China by
430 10.3% based on YIBs offline simulations in the absence of feedbacks from O₃ vegetation
431 damage to meteorology and plant growth. The damage is stronger in summer, when the
432 average GPP decreases by ~20% for both deciduous trees and C3 herbs in the East (Fig.
433 6). In contrast, a lower average damage to GPP of ~10% is predicted for evergreen
434 needleleaf trees (because of low sensitivity) and C4 herbs (because of the mismatched
435 spatial locations between C4 plants and high [O₃], Fig. S1 and Fig. 2d).

436

437 O₃ damage to photosynthesis can influence plant growth. At the same time, the O₃-induced
438 reductions in stomatal conductance (Fig. S6a) can increase canopy temperature and inhibit
439 plant transpiration, leading to surface warming (Fig. S6b), dry air (Fig. S6c), and rainfall
440 deficit (Fig. S6d). These biometeorological feedbacks may in turn exacerbate the
441 dampening of land carbon uptake. Application of ModelE2-YIBs that allows for these
442 feedbacks gives an O₃-induced damage to annual GPP of 10.7%, a similar level to the
443 damage computed in YIBs offline. ~~The spatial pattern of the online O₃ inhibition also
444 resembles that of offline damages (not shown). Sensitivity simulations with zero
445 anthropogenic emissions show almost no O₃ damage (Fig. S7), because the [O₃] exposure
446 from natural sources alone is usually lower than the threshold level of 40 ppbv below which
447 the damage for most PFTs is limited (Fig. 5). Our results indicate that present-day surface
448 O₃ causes strong inhibitions on total NPP in China, ranging from 0.43 ± 0.12 Pg C yr⁻¹ with
449 low sensitivity to 0.76 ± 0.15 Pg C yr⁻¹ with high sensitivity (Table 3). The central value
450 of NPP reduction by O₃ is 0.59 ± 0.11 Pg C yr⁻¹, assuming no direct impacts of O₃ on plant~~

Deleted: (Lombardozzi et al., 2015),

Deleted: S6

Deleted: Sensitivity simulations (

Deleted: and online)

Deleted: ,

Deleted: damaging

Deleted: inhibition, averaged for low and high plant sensitivities, reduces

Deleted: (Table 2),

460 respiration. About 61% of such inhibition occurs in summer, when both photosynthesis
461 and [O₃] reach maximum of the year.

462

463 3.3 Aerosol haze effects in China

464

465 Aerosols decrease direct solar radiation but increase diffuse radiation (Fig. S8), the latter
466 of which is beneficial for canopy photosynthesis. The online-coupled model quantifies the
467 concomitant meteorological and hydrological feedbacks (Fig. 7) that further influence the
468 radiative and land carbon fluxes. Reduced insolation decreases summer surface
469 temperature by 0.63°C in the East, inhibiting evaporation but increasing relative humidity
470 (RH) due to the lower saturation vapor pressure (Table S5). These feedbacks combine to
471 stimulate photosynthesis (Fig. 8a), which, in turn, strengthens plant transpiration (not
472 shown). Atmospheric circulation and moisture convergence are also altered due to the
473 pollution-vegetation-climate interactions, resulting in enhanced precipitation (Fig. 7b) and
474 cloud cover (Fig. 7d). Moreover, soil moisture increases (Fig. 7f) with lower evaporation
475 (Fig. 7e) and higher precipitation (Fig. 7b). Inclusion of AIE results in distinct climatic
476 feedbacks (Fig. S9). Summer precipitation decreases by 0.9 mm day⁻¹ (13%), leading to a
477 3% decline in soil moisture (Table S6). The AIE lengthens cloud lifetime and increases
478 cloud cover, further reducing available radiation and causing a stronger surface cooling.
479 Compared to aerosol-induced perturbations in radiation and temperature, responses in
480 hydrological variables (e.g. precipitation and soil moisture) are usually statistically
481 insignificant on the domain average due to the large relative interannual climate variability
482 (Tables S5 and S6). The resulting meteorological changes over China are a combination of
483 locally driven effects (such as changes in radiation and hence temperature) and regional-
484 globally driven effects (such as changes in rainfall and hence soil water).

485

486 We separate the relative impacts due to aerosol-induced perturbations in temperature,
487 radiation, and soil moisture (Fig. 8). The overall impact of the aerosol-induced
488 biometeorological feedbacks on the carbon uptake depends on the season and vegetation
489 type. In the summer, the aerosol-induced surface cooling brings leaf temperature closer to
490 the photosynthetic optimum of 25°C, DRF enhances light availability of shaded leaves and

Deleted: S7

Deleted:

Deleted: S6

Deleted: further increases RH, contributing

Deleted: .

Deleted: .

Deleted: S8). The AIE reduces cloud droplet size and inhibits summer

Deleted: also

500 LUE of sunlit leaves, and the wetter soil alleviates water stress for stoma. Consequently,
501 aerosol-induced hydroclimatic feedbacks promote ecosystem NPP, albeit with substantial
502 spatiotemporal variability (Fig. 8a and Table 3). Surface cooling enhances NPP in summer
503 (Fig. 8b) but induces neutral net impacts on NPP in spring and autumn (not shown), when
504 leaf temperature is usually below 25°C, because the cooling-driven reductions of
505 photosynthesis are accompanied by simultaneous reductions in plant respiration. We find
506 strong aerosol DRF in the Southeast and the Northeast, where AOD is moderate (Fig. 8c).
507 Over the North China Plain and the Southwest, aerosol DRF is more limited. In these
508 regions, the local background aerosol layer and/or cloud over are sufficiently optically
509 thick that the effect of anthropogenic aerosol pollution is largely to attenuate direct sunlight
510 and reduce NPP (Cohan et al., 2002). Aerosol-induced cooling increases soil moisture over
511 most of the East (Fig. 7f), but the beneficial responses are confined to the Central East (Fig.
512 8d), where C3 crops dominate (Fig. S1). These short-root plants are more sensitive to short-
513 term water availability than deep-root trees (Beer et al., 2010; Yue et al., 2015).

Deleted: 2

Deleted: Plant phenology is responding to aerosol-induced cooling; however, such changes alone exert much smaller impacts on the ecosystem carbon uptake compared to those driven directly by temperature changes (Yue et al., 2015).

514
515 In contrast, inclusion of AIE results in detrimental impacts on NPP (Table 3). Aerosol-
516 induced drought strongly reduces regional NPP especially over the Northeast and North
517 China Plain (Fig. S10d), where cropland dominates (Fig. S1). Meanwhile, the increases in
518 cloud cover reduce available radiation, leading to weakened aerosol DRF effects over the
519 Southeast while strengthened NPP reductions in the Southwest (Fig. S10c).

Deleted: 2

Deleted: S9d

Deleted: S9c

521 3.4 Combined effects of O₃ and aerosol

522
523 Simultaneous inclusion of the aerosol effects on the land biosphere has negligible impacts
524 on O₃ damage. The online O₃ inhibition, which is much stronger in magnitude than the
525 aerosol effects, shows insignificant differences relative to the offline values (10.7% vs.
526 10.3%). As a result, we consider O₃ and aerosol effects to be linearly additive. In the year
527 2010, the combined effects of O₃ and aerosols (Table 3) decrease total NPP in China by
528 0.39 (without AIE) to 0.80 Pg C yr⁻¹ (with AIE), equivalent to 9-16% of the pollution-free
529 NPP and 16-32% of the total anthropogenic carbon emissions (Liu et al., 2015). Spatially,
530 a dominant fraction (86% without AIE and 77% with AIE) of the reduced carbon uptake

Deleted: Table 2

Deleted: A

541 occurs in the East, where dense air pollution is co-located with high NPP (Figs 1 and 2).
542 Temporally, a dominant fraction (60% without AIE and 52% with AIE) of the reduced
543 carbon uptake occurs in summer, when both NPP and [O₃] reach maximum of the year.
544 Independently, O₃ reduces NPP by 0.59 Pg C yr⁻¹, with a large range from 0.43 Pg C yr⁻¹
545 for low damaging sensitivity to 0.76 Pg C yr⁻¹ for high damaging sensitivity (Table 3). The
546 sign of the aerosol effects is uncertain. Without AIE, aerosol is predicted to increase NPP
547 by 0.2 Pg C yr⁻¹, because of regionally confined DRF effects and enhanced soil moisture
548 (Fig. 8). With inclusion of AIE, aerosol decreases NPP by 0.2 Pg C yr⁻¹, mainly due to
549 reduced soil moisture (Fig. S10). The uncertainty of individual simulations, calculated
550 from the interannual climate variability, is usually smaller than that due to O₃ damage
551 sensitivity and AIE (Table 3).

Deleted: 2

Deleted: S9

Deleted: 2

553 3.5 Future projection of pollution effects

554
555 Following the CLE scenario, by the year 2030, predicted summer [O₃] increases by 7%,
556 while AOD decreases by 5% and surface PM_{2.5} concentrations decline by 10% (Fig. 9).
557 These changes are predominantly attributed to changes in anthropogenic emissions, as
558 natural sources show limited changes. The reduction of AOD is related to the decreased
559 emissions of SO₂, black carbon, and organic carbon (Fig. S2). In contrast, the enhancement
560 of [O₃] results from the increased NO_x emissions, higher level of background CH₄ (~20%),
561 and higher air temperature in the warmer 2030 climate. The moderate decline of aerosol
562 loading in the 2030 CLE scenario brings benefits to land ecosystems through DRF effects
563 (Table 3) because light scattering is often saturated in the present-day conditions due to
564 high local AOD and regional cloud cover. Benefits from the aerosol pollution reductions
565 are offset by worsening O₃ vegetation damage in the CLE future world (Fig. 10b). O₃-free
566 ([O₃]=0) NPP increases by 14% in 2030 due to CO₂ fertilization and global climate change.
567 Despite [CO₂] increases from 390 ppm in 2010 to 449 ppm in 2030 in the RCP8.5 scenario
568 (van Vuuren et al., 2011), which contributes to g_s inhibition of 4% on the country level, the
569 future O₃-induced NPP damage in 2030 degrades to 14% or 0.67 Pg C yr⁻¹ (Table 3), with
570 a range from 0.43 Pg C yr⁻¹ (low O₃ sensitivity) to 0.90 Pg C yr⁻¹ (high O₃ sensitivity).

Deleted: is caused by

Deleted: NO_x accompanied with the

Deleted: 2

Deleted: drives additional

Deleted: 2

580 The MTFR scenario reflects an ambitious and optimistic future in which there is rapid
581 global implementation of all currently available technological pollution controls. AOD
582 decreases by 55% and [O₃] decreases by 40% for this future scenario (Fig. 9). The model
583 projects much lower damage to NPP of only 0.12 Pg C yr⁻¹ ~~with a range from 0.06 Pg C~~
584 ~~yr⁻¹ (low O₃ sensitivity) to 0.20 Pg C yr⁻¹ (high O₃ sensitivity), mainly due to the 40%~~
585 ~~reduction in [O₃] (Fig. 10c). Including both aerosol direct and indirect effects, O₃ and~~
586 ~~aerosols together inhibit future NPP by 0.28 Pg C yr⁻¹, ranging from 0.12 Pg C yr⁻¹ with~~
587 ~~low O₃ sensitivity to 0.43 Pg C yr⁻¹ with high O₃ sensitivity. As a result,~~ The MTFR
588 scenario offers strong recovery of the land carbon uptake in China by 2030.

Deleted: (0.28 Pg C yr⁻¹ with AIE), mainly from the 40% reduction in [O₃] (Fig. 10c). These damages are of similar magnitude to modeling uncertainties (Table 2).

589

590 4. Discussion

591

592 4.1 Comparison with previous estimates

593

594 Previous estimates of O₃ damages over the whole China region are very limited. Two
595 important studies, Tian et al. (2011) and Ren et al. (2011), have quantified the impacts of
596 surface O₃ on carbon assimilation in China. Both studies applied the dynamic land
597 ecosystem model (DLEM) with O₃ damage scheme proposed by Felzer et al. (2004), except
598 that Tian et al. (2011) focused on NEE while Ren et al. (2011) also investigated NPP. The
599 Felzer et al. (2004) scheme calculates O₃ uptake based on stomatal conductance and the
600 AOT40 (accumulated hourly O₃ dose over a threshold of 40 ppb). Yue and Unger (2014)
601 estimated O₃-induced reductions in GPP over U.S. using Sitch et al. (2007) scheme and
602 found an average value of 4-8% (low to high sensitivity), consistent with the reduction of
603 3-7% in Felzer et al. (2004). For this study, we estimate that present-day O₃ decreases NPP
604 by 0.43-0.76 Pg C yr⁻¹, higher than the 0.42 Pg C yr⁻¹ calculated by Ren et al. (2011).
605 However, the percentage reduction of 10.1-17.8% in our estimate is weaker than the value
606 of 24.7% in Ren et al. (2011). The main reason for such discrepancy lies in the differences
607 in the climatological NPP. Combining all environmental drivers (e.g. [CO₂], meteorology,
608 [O₃], and aerosols), we predict an average NPP of 3.98 ± 0.1 Pg C yr⁻¹ for the year 2010
609 (uncertainties from AIE) with the ModelE2-YIBs model. This value is close to the average
610 of 3.35 ± 1.25 Pg C yr⁻¹ for 1981-2000 calculated based on 54 estimates from 33 studies

Deleted: ±

Deleted: ±

616 (Shao et al., 2016). Using DLEM, Ren et al. (2011) estimated an optimal NPP of 1.67 Pg
617 C yr⁻¹ for 2000-2005 over China, which is only half of the literature-based estimate.

618

619 In the absence of any previous studies of aerosol pollution effects on land carbon uptake in
620 China, our strategy is to compare separately the simulated aerosol climatic feedback
621 (climate sensitivity) and simulated NPP response to climate variability (NPP sensitivity)
622 with existing published results. ModelE2-YIBs simulates an annual reduction of 26.2 W
623 m⁻² in all-sky surface solar radiation over the East due to aerosols pollution (Table S5),
624 similar to the estimate of 28 W m⁻² by Folini and Wild (2015). In response to this radiative
625 perturbation, aerosol pollution causes a widespread cooling of 0.3-0.9 °C in summer over
626 the East (Fig. 7a), consistent with estimates of 0-0.9 °C by Qian et al. (2003), 0-0.7 °C by
627 Liu et al. (2009), and average of 0.5 °C by Folini and Wild (2015). Aerosol pollution effects
628 on regional precipitation patterns in China are not well understood due to different climate
629 model treatments of land-atmosphere interactions and the interplay between regional and
630 large-scale circulation. In ModelE2-YIBs, without AIE, aerosol induces a “northern
631 drought and southern flood” pattern in agreement with Gu et al. (2006), but different to Liu
632 et al. (2009) who predicted widespread drought instead. Including both aerosol direct and
633 indirect effects, ModelE2-YIBs simulates an average reduction of 0.48 mm day⁻¹ in
634 summer rainfall widespread over China (Fig. S9b), similar to the magnitude of 0.4 mm
635 day⁻¹ estimated with the ECHAM5-HAM model (Folini and Wild, 2015), but higher than
636 the 0.21 mm day⁻¹ predicted by the RegCM2 model (Huang et al., 2007).

637

638 Sensitivity experiments with YIBs show that summer NPP increases following aerosol-
639 induced changes in temperature, radiation, and precipitation (Fig. 8). The cooling-related
640 NPP enhancement (Fig. 8b) collocates with changes in temperature (Fig. 7a), indicating
641 that sensitivity of NPP to temperature is negative over eastern China. Such temperature
642 sensitivity is consistent with the ensemble estimate based on 10 terrestrial models (Piao et
643 al., 2013). For the aerosol-induced radiative perturbation, many studies have shown that
644 moderate aerosol/cloud amount promotes plant photosynthesis through enhanced DRF,
645 while dense aerosol/cloud decreases carbon uptake due to light extinction (Cohan et al.,
646 2002; Gu et al., 2003; Rocha et al., 2004; Alton, 2008; Knohl and Baldocchi, 2008;

Deleted: S6

Deleted: S8b

649 Mercado et al., 2009; Jing et al., 2010; Bai et al., 2012; Cirino et al., 2014; Strada et al.,
650 2015). Theoretically, at each specific land location on the Earth, there is an AOD threshold
651 below which aerosol promotes local NPP. The threshold is dependent on latitude,
652 cloud/aerosol amount, and plant types. In a related study by [Yue and Unger \(2017\)](#), we
653 applied a well-validated offline radiation model to calculate these AOD thresholds over
654 China. We conclude that present-day AOD is lower than the local thresholds in the
655 Northeast and Southeast but exceeds the thresholds in the North China Plain, explaining
656 why aerosol-induced diming enhances NPP in the former regions but reduces NPP in the
657 latter (Fig. 8c). On the country level, the NPP enhancement due to aerosol DRF is 0.07 Pg
658 C yr⁻¹ in [Yue and Unger \(2017\)](#), very close to the 0.09 Pg C yr⁻¹ estimated with ModelE2-
659 [YIBs model \(Table 2\)](#).

Deleted: Yue and Unger (2016)

Deleted: Yue and Unger (2016), very close to the 0.09 Pg C yr⁻¹ estimated with ModelE2-YIBs model (Table 2).

661 4.2 Uncertainties

662
663 A major source of uncertainty originates from the paucity of observations. For instance,
664 direct measurements of aerosol pollution effects on NPP are non-existent for China. The
665 aerosol effects involve complex interactions that challenge the field-based validation of the
666 underlying independent processes. Field experiments of O₃ vegetation damage are
667 becoming more available, but their applications are limited by the large variations in the
668 species-specific responses (Lombardozi et al., 2013), as well as the discrepancies in the
669 treatments of [O₃] enhancement (Wittig et al., 2007). Instead of equally using all individual
670 records from multiple literatures (Lombardozi et al., 2013), we aggregate O₃ damage for
671 each literature based on the seasonal (or growth-season) average. In this way, the derived
672 PFT-level GPP-[O₃] relationships are not biased towards the experiments with a large
673 number of samplings. Such aggregation also reduces sampling noise and allows
674 construction of the quantified GPP-[O₃] relationships used for model assessment. [Predicted](#)
675 [\[O₃\] is largely overestimated at urban sites but exhibits reasonable magnitude at rural sites](#)
676 [\(Figs 2 and 3\). Measurements of background \[O₃\] in China are limited both in space and](#)
677 [time, restricting comprehensive validation of \[O₃\] and the consequent estimate of O₃](#)
678 [damages on the country level.](#)

679

683 We have estimated O₃ damages to NPP (instead of GPP), an optimal indicator for net
684 carbon uptake by plants. Our calculations assume no impacts of O₃ on autotrophic
685 respiration. Yet, limited observations have found increased plant respiration in response to
686 O₃ injury (Felzer et al., 2007), suggesting that our calculation of O₃-induced NPP
687 reductions might be underestimated. Current large mechanistic uncertainties in the role of
688 anthropogenic nitrogen (N) deposition to China's land carbon uptake (Tian et al., 2011;
689 Xiao et al., 2015) have prohibited the inclusion of dynamic carbon-nitrogen coupling in
690 the Earth system model used here. Previous studies have suggested that inclusion of N
691 fertilization can relieve or offset damages by O₃, especially for N-limited forests (Ollinger
692 et al., 2002). Relative to the present day, atmospheric reactive N deposition increases by
693 20% in the CLE scenario but decreases by 60% in the MTFR scenario, suggesting that the
694 stronger O₃ damage in CLE might be overestimated while the reduced damage in MTFR
695 might be too optimistic. ▽

Deleted: Furthermore, the relatively coarse resolution of the global model, usage of emission inventories, selection of aerosol parameters, and application of AIE

696
697 Our estimate of NPP responses to aerosol pollution is sensitive to modeling uncertainties
698 in concentration, radiation, and climatic effects. Simulated surface PM_{2.5} is reasonable but
699 AOD is underestimated in the North China Plain (Fig. 2), likely because of the biases in
700 aerosol optical parameters. Using a different set of optical parameters, we predicted much
701 higher AOD that is closer to observations with the same aerosol vertical profile and particle
702 compositions (Yue and Unger, 2017). The model overestimates diffuse fraction in China
703 (Fig. 4), likely because of simulated biases in clouds. Previously, we improved the
704 prediction of diffuse fraction in China using observed cloud profiles for the region (Yue
705 and Unger, 2017). Biases in simulated AOD and diffuse fraction introduce uncertainties in
706 the aerosol DRF especially in the affected localized model grid cells. Yet, averaged over
707 the China domain, our estimate of NPP change by aerosol DRF (0.09 Pg C yr⁻¹) is
708 consistent with the previous assessment in Yue and Unger (2017) (0.07 Pg C yr⁻¹). Aerosol-
709 induced impacts on precipitation and soil moisture are not statistically significant over the
710 regionally averaged domain (Tables S5 and S6). However, for the 2010 and 2030 CLE
711 cases with AIE, 2 out of 6 scenarios, the aerosol-induced impact on soil moisture dominates
712 the total NPP response (Table 3). Furthermore, the relatively coarse resolution of the global

716 model and usage of emission inventories may introduce additional biases and exacerbate
717 the total uncertainties.

718

719 Importantly, our estimate of NPP response to aerosol effects, with or without AIE, is
720 secondary in magnitude compared ~~to the O₃ vegetation damage, suggesting that the net~~
721 impact of current air pollution levels in China is detrimental to the land carbon uptake
722 there. Locally, this pollution damage exerts a threat to plant health, terrestrial ecosystem
723 services, and food production. Globally, air pollution effects may enhance planetary
724 warming by decreasing the land removal rate of atmospheric CO₂. Our results show
725 substantial benefits to the protection of plant health and the regional land carbon sink in
726 China from stringent air pollution controls, especially for O₃ precursors. Our analysis
727 highlights the complex interplay between immediate and more local pollution issues, and
728 longer-term global warming. Future air pollution controls provide an additional co-benefit
729 to human society: the offsetting of fossil fuel CO₂ emissions through enhanced land
730 sequestration of atmospheric CO₂.

731

732 *Acknowledgements.* The authors are grateful to Prof. William Collins and an anonymous
733 reviewer for constructive comments improving this paper. X. Yue acknowledges funding
734 support from the National Basic Research Program of China (973 program, Grant No.
735 2014CB441202) and the “Thousand Youth Talents Plan”. This research was supported in
736 part by the facilities and staff of the Yale University Faculty of Arts and Sciences High
737 Performance Computing Center.

738

739

Deleted: with

741 **References**

- 742 Ainsworth, E. A., Yendrek, C. R., Sitch, S., Collins, W. J., and Emberson, L. D.: The
743 Effects of Tropospheric Ozone on Net Primary Productivity and Implications for
744 Climate Change, *Annual Review of Plant Biology*, Vol 63, 63, 637-661,
745 doi:10.1146/Annurev-Arplant-042110-103829, 2012.
- 746 Alton, P. B.: Reduced carbon sequestration in terrestrial ecosystems under overcast skies
747 compared to clear skies, *Agricultural and Forest Meteorology*, 148, 1641–1653,
748 doi:10.1016/j.agrformet.2008.05.014, 2008.
- 749 Amann, M., Bertok, I., Borcken-Kleefeld, J., Cofala, J., Heyes, C., Hoglund-Isaksson, L.,
750 Klimont, Z., Nguyen, B., Posch, M., Rafaj, P., Sandler, R., Schopp, W., Wagner, F.,
751 and Winiwarter, W.: Cost-effective control of air quality and greenhouse gases in
752 Europe: Modeling and policy applications, *Environmental Modelling & Software*,
753 26, 1489-1501, doi:10.1016/j.envsoft.2011.07.012, 2011.
- 754 Bai, Y., Wang, J., Zhang, B., Zhang, Z., and Liang, J.: Comparing the impact of
755 cloudiness on carbon dioxide exchange in a grassland and a maize cropland in
756 northwestern China, *Ecological Research*, 27, 615-623, doi:10.1007/s11284-012-
757 0930-z, 2012.
- 758 Ball, J. T., Woodrow, I. E., and Berry, J. A.: A model predicting stomatal conductance
759 and its contribution to the control of photosynthesis under different environmental
760 conditions, in: *Progress in Photosynthesis Research*, edited by: Biggins, J., Nijhoff,
761 Dordrecht, Netherlands, 110–112, 1987.
- 762 Bauer, S. E., Mishchenko, M. I., Laci, A. A., Zhang, S., Perlwitz, J., and Metzger, S. M.:
763 Do sulfate and nitrate coatings on mineral dust have important effects on radiative
764 properties and climate modeling?, *Journal of Geophysical Research*, 112, D06307
765 doi:10.1029/2005JD006977, 2007.
- 766 Beer, C., Reichstein, M., Tomelleri, E., Ciais, P., Jung, M., Carvalhais, N., Rodenbeck,
767 C., Arain, M. A., Baldocchi, D., Bonan, G. B., Bondeau, A., Cescatti, A., Lasslop,
768 G., Lindroth, A., Lomas, M., Luysaert, S., Margolis, H., Oleson, K. W., Roupsard,
769 O., Veenendaal, E., Viovy, N., Williams, C., Woodward, F. I., and Papale, D.:
770 Terrestrial Gross Carbon Dioxide Uptake: Global Distribution and Covariation with
771 Climate, *Science*, 329, 834-838, doi:10.1126/Science.1184984, 2010.
- 772 Cirino, G. G., Souza, R. A. F., Adams, D. K., and Artaxo, P.: The effect of atmospheric
773 aerosol particles and clouds on net ecosystem exchange in the Amazon, *Atmospheric
774 Chemistry and Physics*, 14, 6523-6543, doi:10.5194/acp-14-6523-2014, 2014.
- 775 Cohan, D. S., Xu, J., Greenwald, R., Bergin, M. H., and Chameides, W. L.: Impact of
776 atmospheric aerosol light scattering and absorption on terrestrial net primary
777 productivity, *Global Biogeochemical Cycles*, 16, 1090, doi:10.1029/2001gb001441,
778 2002.
- 779 Defries, R. S., Hansen, M. C., Townshend, J. R. G., Janetos, A. C., and Loveland, T. R.:
780 A new global 1-km dataset of percentage tree cover derived from remote sensing,
781 *Global Change Biology*, 6, 247-254, doi:10.1046/J.1365-2486.2000.00296.X, 2000.
- 782 Farquhar, G. D., Caemmerer, S. V., and Berry, J. A.: A Biochemical-Model of
783 Photosynthetic Co₂ Assimilation in Leaves of C-3 Species, *Planta*, 149, 78-90,
784 doi:10.1007/Bf00386231, 1980.
- 785 Felzer, B., Kicklighter, D., Melillo, J., Wang, C., Zhuang, Q., and Prinn, R.: Effects of
786 ozone on net primary production and carbon sequestration in the conterminous

787 United States using a biogeochemistry model, *Tellus Series B-Chemical and*
788 *Physical Meteorology*, 56, 230-248, doi:Doi 10.1111/J.1600-0889.2004.00097.X,
789 2004.

790 Felzer, B. S., Cronin, T., Reilly, J. M., Melillo, J. M., and Wang, X.: Impacts of ozone on
791 trees and crops, *C. R. Geoscience*, 229, doi:10.1016/j.crte.2007.08.008, 2007.

792 Folini, D., and Wild, M.: The effect of aerosols and sea surface temperature on China's
793 climate in the late twentieth century from ensembles of global climate simulations, *J.*
794 *Geophys. Res.*, 12, 2261-2279, doi:10.1002/2014JD022851, 2015.

795 Gu, L. H., Baldocchi, D. D., Wofsy, S. C., Munger, J. W., Michalsky, J. J., Urbanski, S.
796 P., and Boden, T. A.: Response of a deciduous forest to the Mount Pinatubo
797 eruption: Enhanced photosynthesis, *Science*, 299, 2035-2038,
798 doi:10.1126/science.1078366, 2003.

799 Gu, Y., Liou, K. N., Xue, Y., Mechoso, C. R., Li, W., and Luo, Y.: Climatic effects of
800 different aerosol types in China simulated by the UCLA general circulation model,
801 *Journal of Geophysical Research*, 111, D15201, doi:10.1029/2005JD006312, 2006.

802 Hansen, M. C., DeFries, R. S., Townshend, J. R. G., Carroll, M., Dimiceli, C., and
803 Sohlberg, R. A.: Global Percent Tree Cover at a Spatial Resolution of 500 Meters:
804 First Results of the MODIS Vegetation Continuous Fields Algorithm, *Earth*
805 *Interactions*, 7, 1-15, doi:10.1175/1087-3562(2003)007<0001:GPTCAA>2.0.CO;2,
806 2003.

807 Huang, Y., Chameides, W. L., and Dickinson, R. E.: Direct and indirect effects of
808 anthropogenic aerosols on regional precipitation over east Asia, *Journal of*
809 *Geophysical Research*, 112, D03212, doi:10.1029/2006JD007114, 2007.

810 Jing, X., Huang, J., Wang, G., Higuchi, K., Bi, J., Sun, Y., Yu, H., and Wang, T.: The
811 effects of clouds and aerosols on net ecosystem CO₂ exchange over semi-arid Loess
812 Plateau of Northwest China, *Atmospheric Chemistry and Physics*, 10, 8205-8218,
813 doi:10.5194/acp-10-8205-2010, 2010.

814 Jung, M., Reichstein, M., and Bondeau, A.: Towards global empirical upscaling of
815 FLUXNET eddy covariance observations: validation of a model tree ensemble
816 approach using a biosphere model, *Biogeosciences*, 6, 2001-2013, doi:10.5194/bg-6-
817 2001-2009, 2009.

818 Kanniah, K. D., Beringer, J., North, P., and Hutley, L.: Control of atmospheric particles
819 on diffuse radiation and terrestrial plant productivity: A review, *Progress in Physical*
820 *Geography*, 36, 209-237, doi:10.1177/0309133311434244, 2012.

821 Knohl, A., and Baldocchi, D. D.: Effects of diffuse radiation on canopy gas exchange
822 processes in a forest ecosystem, *Journal of Geophysical Research*, 113, G02023,
823 doi:10.1029/2007JG000663, 2008.

824 Liu, Y., Sun, J., and Yang, B.: The effects of black carbon and sulphate aerosols in China
825 regions on East Asia monsoons, *Tellus Series B-Chemical and Physical*
826 *Meteorology*, 61B, 642-656, doi:10.1111/j.1600-0889.2009.00427.x, 2009.

827 Liu, Z., Guan, D. B., Wei, W., Davis, S. J., Ciais, P., Bai, J., Peng, S. S., Zhang, Q.,
828 Hubacek, K., Marland, G., Andres, R. J., Crawford-Brown, D., Lin, J. T., Zhao, H.
829 Y., Hong, C. P., Boden, T. A., Feng, K. S., Peters, G. P., Xi, F. M., Liu, J. G., Li, Y.,
830 Zhao, Y., Zeng, N., and He, K. B.: Reduced carbon emission estimates from fossil
831 fuel combustion and cement production in China, *Nature*, 524, 335-338,
832 doi:10.1038/nature14677, 2015.

833 Lombardozzi, D., Sparks, J. P., and Bonan, G.: Integrating O₃ influences on terrestrial
834 processes: photosynthetic and stomatal response data available for regional and
835 global modeling, *Biogeosciences*, 10, 6815-6831, doi:10.5194/bg-10-6815-2013,
836 2013.

837 ~~Menon, S., and Rotstayn, L.: The radiative influence of aerosol effects on liquid-phase
838 cumulus and stratiform clouds based on sensitivity studies with two climate models,
839 *Climate Dynamics*, 27, 345-356, doi:10.1007/s00382-006-0139-3, 2006.~~

840 Mercado, L. M., Bellouin, N., Sitch, S., Boucher, O., Huntingford, C., Wild, M., and
841 Cox, P. M.: Impact of changes in diffuse radiation on the global land carbon sink,
842 *Nature*, 458, 1014-1017, doi:10.1038/Nature07949, 2009.

843 Oleson, K. W., Lawrence, D. M., Bonan, G. B., Flanner, M. G., Kluzek, E., Lawrence, P.
844 J., Levis, S., Swenson, S. C., and Thornton, P. E.: Technical Description of version
845 4.0 of the Community Land Model (CLM), National Center for Atmospheric
846 Research, Boulder, CONCAR/TN-478+STR, 2010.

847 Ollinger, S. V., Aber, J. D., Reich, P. B., and Freuder, R. J.: Interactive effects of
848 nitrogen deposition, tropospheric ozone, elevated CO₂ and land use history on the
849 carbon dynamics of northern hardwood forests, *Global Change Biology*, 8, 545-562,
850 doi:10.1046/J.1365-2486.2002.00482.X, 2002.

851 Piao, S. L., Fang, J. Y., Ciais, P., Peylin, P., Huang, Y., Sitch, S., and Wang, T.: The
852 carbon balance of terrestrial ecosystems in China, *Nature*, 458, 1009-1013,
853 doi:10.1038/nature07944, 2009.

854 Piao, S. L., Sitch, S., Ciais, P., Friedlingstein, P., Peylin, P., Wang, X. H., Ahlstrom, A.,
855 Anav, A., Canadell, J. G., Cong, N., Huntingford, C., Jung, M., Levis, S., Levy, P.
856 E., Li, J. S., Lin, X., Lomas, M. R., Lu, M., Luo, Y. Q., Ma, Y. C., Myneni, R. B.,
857 Poulter, B., Sun, Z. Z., Wang, T., Viovy, N., Zaehle, S., and Zeng, N.: Evaluation of
858 terrestrial carbon cycle models for their response to climate variability and to CO₂
859 trends, *Global Change Biology*, 19, 2117-2132, doi:10.1111/Gcb.12187, 2013.

860 Pickering, K. E., Wang, Y., Tao, W.-K., Price, C., and Müller, J.-F.: Vertical distributions
861 of lightning NO_x for use in regional and global chemical transport models, *Journal of*
862 *Geophysical Research*, 103, 31203–31216, doi:10.1029/98JD02651, 1998.

863 Price, C., Penner, J., and Prather, M.: NO_x from lightning: 1. Global distribution based
864 on lightning physics, *Journal of Geophysical Research*, 102, 5929–5941,
865 doi:10.1029/96JD03504, 1997.

866 Qian, Y., Leung, L. R., Ghan, S. J., and Giorgi, F.: Regional climate effects of aerosols
867 over China: modeling and observation, *Tellus Series B-Chemical and Physical*
868 *Meteorology*, 55, 914-934, doi:10.1046/j.1435-6935.2003.00070.x, 2003.

869 Reich, P. B., and Amundson, R. G.: Ambient Levels of Ozone Reduce Net
870 Photosynthesis in Tree and Crop Species, *Science*, 230, 566-570,
871 doi:10.1126/science.230.4725.566, 1985.

872 Ren, W., Tian, H., Tao, B., Chappelka, A., Sun, G., Lu, C., Liu, M., Chen, G., and Xu,
873 X.: Impacts of tropospheric ozone and climate change on net primary productivity
874 and net carbon exchange of China's forest ecosystems, *Global Ecology &*
875 *Biogeography*, 20, 391-406, doi:10.1111/j.1466-8238.2010.00606.x, 2011.

876 Rienecker, M. M., Suarez, M. J., Gelaro, R., Todling, R., Bacmeister, J., Liu, E.,
877 Bosilovich, M. G., Schubert, S. D., Takacs, L., Kim, G. K., Bloom, S., Chen, J. Y.,
878 Collins, D., Conaty, A., Da Silva, A., Gu, W., Joiner, J., Koster, R. D., Lucchesi, R.,

Deleted: Lombardozzi, D., Levis, S., Bonan, G., Hess, P. G., and Sparks, J. P.: The Influence of Chronic Ozone Exposure on Global Carbon and Water Cycles, *Journal of Climate*, 28, 292-305, doi:10.1175/Jcli-D-14-00223.1, 2015.

883 Molod, A., Owens, T., Pawson, S., Pegion, P., Redder, C. R., Reichle, R., Robertson,
884 F. R., Ruddick, A. G., Sienkiewicz, M., and Woollen, J.: MERRA: NASA's Modern-
885 Era Retrospective Analysis for Research and Applications, *Journal of Climate*, 24,
886 3624-3648, doi:10.1175/Jcli-D-11-00015.1, 2011.

887 Rocha, A. V., Su, H. B., Vogel, C. S., Schmid, H. P., and Curtis, P. S.: Photosynthetic
888 and water use efficiency responses to diffuse radiation by an aspen-dominated
889 northern hardwood forest, *Forest Science*, 50, 793-801, 2004.

890 Schaefer, K., Schwalm, C. R., Williams, C., Arain, M. A., Barr, A., Chen, J. M., Davis,
891 K. J., Dimitrov, D., Hilton, T. W., Hollinger, D. Y., Humphreys, E., Poulter, B.,
892 Raczka, B. M., Richardson, A. D., Sahoo, A., Thornton, P., Vargas, R., Verbeeck,
893 H., Anderson, R., Baker, I., Black, T. A., Bolstad, P., Chen, J. Q., Curtis, P. S.,
894 Desai, A. R., Dietze, M., Dragoni, D., Gough, C., Grant, R. F., Gu, L. H., Jain, A.,
895 Kucharik, C., Law, B., Liu, S. G., Lokipitiya, E., Margolis, H. A., Matamala, R.,
896 McCaughey, J. H., Monson, R., Munger, J. W., Oechel, W., Peng, C. H., Price, D.
897 T., Ricciuto, D., Riley, W. J., Roulet, N., Tian, H. Q., Tonitto, C., Torn, M., Weng,
898 E. S., and Zhou, X. L.: A model-data comparison of gross primary productivity:
899 Results from the North American Carbon Program site synthesis, *J. Geophys. Res.*,
900 117, G03010, doi:10.1029/2012jg001960, 2012.

901 Schmidt, G. A., Kelley, M., Nazarenko, L., Ruedy, R., Russell, G. L., Aleinov, I., Bauer,
902 M., Bauer, S. E., Bhat, M. K., Bleck, R., Canuto, V., Chen, Y. H., Cheng, Y., Clune,
903 T. L., Del Genio, A., de Fainchtein, R., Faluvegi, G., Hansen, J. E., Healy, R. J.,
904 Kiang, N. Y., Koch, D., Lacis, A. A., LeGrande, A. N., Lerner, J., Lo, K. K.,
905 Matthews, E. E., Menon, S., Miller, R. L., Oinas, V., Oloso, A. O., Perlwitz, J. P.,
906 Puma, M. J., Putman, W. M., Rind, D., Romanou, A., Sato, M., Shindell, D. T., Sun,
907 S., Syed, R. A., Tausnev, N., Tsigaridis, K., Unger, N., Voulgarakis, A., Yao, M. S.,
908 and Zhang, J. L.: Configuration and assessment of the GISS ModelE2 contributions
909 to the CMIP5 archive, *Journal of Advances in Modeling Earth Systems*, 6, 141-184,
910 doi:10.1002/2013ms000265, 2014.

911 Shao, J., Zhou, X. H., Luo, Y. Q., Zhang, G. D., Yan, W., Li, J. X., Li, B., Dan, L.,
912 Fisher, J. B., Gao, Z. Q., He, Y., Huntzinger, D., Jain, A. K., Mao, J. F., Meng, J. H.,
913 Michalak, A. M., Parazoo, N. C., Peng, C. H., Poulter, B., Schwalm, C. R., Shi, X.
914 Y., Sun, R., Tao, F. L., Tian, H. Q., Wei, Y. X., Zeng, N., Zhu, Q., and Zhu, W. Q.:
915 Uncertainty analysis of terrestrial net primary productivity and net biome
916 productivity in China during 1901-2005, *Journal of Geophysical Research*, 121,
917 1372-1393, doi:10.1002/2015jg003062, 2016.

918 [Shindell, D. T., Pechony, O., Voulgarakis, A., Faluvegi, G., Nazarenko, L., Lamarque, J.](#)
919 [F., Bowman, K., Milly, G., Kovari, B., Ruedy, R., and Schmidt, G. A.: Interactive](#)
920 [ozone and methane chemistry in GISS-E2 historical and future climate simulations,](#)
921 [Atmospheric Chemistry and Physics, 13, 2653-2689, doi:10.5194/Acp-13-2653-](#)
922 [2013, 2013.](#)

923 Sitch, S., Cox, P. M., Collins, W. J., and Huntingford, C.: Indirect radiative forcing of
924 climate change through ozone effects on the land-carbon sink, *Nature*, 448, 791-794,
925 doi:10.1038/Nature06059, 2007.

926 Spitters, C. J. T.: Separating the Diffuse and Direct Component of Global Radiation and
927 Its Implications for Modeling Canopy Photosynthesis .2. Calculation of Canopy

928 Photosynthesis, *Agricultural and Forest Meteorology*, 38, 231-242,
929 doi:10.1016/0168-1923(86)90061-4, 1986.

930 Spracklen, D. V., Arnold, S. R., and Taylor, C. M.: Observations of increased tropical
931 rainfall preceded by air passage over forests, *Nature*, 489, 282-285,
932 doi:10.1038/nature11390, 2012.

933 Steiner, A. L., and Chameides, W. L.: Aerosol-induced thermal effects increase modelled
934 terrestrial photosynthesis and transpiration, *Tellus Series B-Chemical and Physical*
935 *Meteorology*, 57, 404-411, doi:DOI 10.1111/j.1600-0889.2005.00158.x, 2005.

936 Strada, S., Unger, N., and Yue, X.: Observed aerosol-induced radiative effect on plant
937 productivity in the eastern United States, *Atmospheric Environment*, 122, 463–476,
938 doi:10.1016/j.atmosenv.2015.09.051, 2015.

939 Tian, H. Q., Melillo, J., Lu, C. Q., Kicklighter, D., Liu, M. L., Ren, W., Xu, X. F., Chen,
940 G. S., Zhang, C., Pan, S. F., Liu, J. Y., and Running, S.: China's terrestrial carbon
941 balance: Contributions from multiple global change factors, *Global Biogeochemical*
942 *Cycles*, 25, Gb1007, doi:10.1029/2010gb003838, 2011.

943 [Unger, N., Harper, K., Zheng, Y., Kiang, N. Y., Aleinov, I., Arneth, A., Schurgers, G.,](#)
944 [Amelynck, C., Goldstein, A., Guenther, A., Heinesch, B., Hewitt, C. N., Karl, T.,](#)
945 [Laffineur, Q., Langford, B., McKinney, K. A., Misztal, P., Potosnak, M., Rinne, J.,](#)
946 [Pressley, S., Schoon, N., and Serça, D.: Photosynthesis-dependent isoprene emission](#)
947 [from leaf to planet in a global carbon–chemistry–climate model, *Atmos. Chem.*](#)
948 [Phys., 13, 17717-17791, doi:10.5194/acp-13-10243-2013, 2013.](#)

949 [Unger, N., and Yue, X.: Strong chemistry-climate feedbacks in the Pliocene, *Geophysical*](#)
950 [Research Letters](#), 41, 527-533, doi:10.1002/2013gl058773, 2014.

951 van Vuuren, D. P., Edmonds, J., Kainuma, M., Riahi, K., Thomson, A., Hibbard, K.,
952 Hurttt, G. C., Kram, T., Krey, V., Lamarque, J. F., Masui, T., Meinshausen, M.,
953 Nakicenovic, N., Smith, S. J., and Rose, S. K.: The representative concentration
954 pathways: an overview, *Climatic Change*, 109, 5-31, doi:10.1007/s10584-011-0148-
955 z, 2011.

956 Wild, M., Folini, D., Schar, C., Loeb, N., Dutton, E. G., and Konig-Langlo, G.: The
957 global energy balance from a surface perspective, *Climate Dynamics*, 40, 3107-3134,
958 doi:10.1007/s00382-012-1569-8, 2013.

959 Wittig, V. E., Ainsworth, E. A., and Long, S. P.: To what extent do current and projected
960 increases in surface ozone affect photosynthesis and stomatal conductance of trees?
961 A meta-analytic review of the last 3 decades of experiments, *Plant Cell and*
962 *Environment*, 30, 1150-1162, doi:10.1111/J.1365-3040.2007.01717.X, 2007.

963 Xia, X.: A closer looking at dimming and brightening in China during 1961-2005,
964 *Annales Geophysicae*, 28, 1121-1132, doi:10.5194/angeo-28-1121-2010, 2010.

965 Xiao, J. F., Zhou, Y., and Zhang, L.: Contributions of natural and human factors to
966 increases in vegetation productivity in China, *Ecosphere*, 6, 233, doi:10.1890/Es14-
967 00394.1, 2015.

968 [Yienger, J. J., and Levy, H.: Empirical-Model of Global Soil-Biogenic Nox Emissions, *J.*](#)
969 [Geophys. Res.](#), 100, 11447-11464, doi:10.1029/95jd00370, 1995.

970 Yue, X., and Unger, N.: Ozone vegetation damage effects on gross primary productivity
971 in the United States, *Atmospheric Chemistry and Physics*, 14, 9137-9153,
972 doi:10.5194/acp-14-9137-2014, 2014.

973 Yue, X., and Unger, N.: The Yale Interactive terrestrial Biosphere model version 1.0:
974 description, evaluation and implementation into NASA GISS ModelE2,
975 Geoscientific Model Development, 8, 2399-2417, doi:10.5194/gmd-8-2399-2015,
976 2015.

977 Yue, X., Unger, N., and Zheng, Y.: Distinguishing the drivers of trends in land carbon
978 fluxes and biogenic emissions over the past three decades, Atmospheric Chemistry
979 and Physics, 15, 11931-11948, doi:10.5194/acp-15-11931-2015, 2015.

980 Yue, X., Keenan, T. F., Munger, W., and Unger, N.: Limited effect of ozone reductions
981 on the 20-year photosynthesis trend at Harvard forest, Global Change Biology, 22,
982 3750-3759, doi:10.1111/gcb.13300, 2016.

983 Yue, X., and Unger, N.: Aerosol optical depth thresholds as a tool to assess diffuse
984 radiation fertilization of the land carbon uptake in China, Atmospheric Chemistry
985 and Physics, 17, 1329-1342, doi:10.5194/acp-17-1329-2017, 2017.

986 Zhao, M. S., Heinsch, F. A., Nemani, R. R., and Running, S. W.: Improvements of the
987 MODIS terrestrial gross and net primary production global data set, Remote Sensing
988 of Environment, 95, 164-176, doi:10.1016/J.Rse.2004.12.011, 2005.

989
990

Deleted: pollution radiative effects on

Deleted: Discussion, in review

Deleted: 2016-899, 2016

994
995
996
997

Table 1. Summary of models and simulations

Model Name	Model class	Climate drivers	Number of runs	Table index ^a	Purpose
ModelE2-YIBs	Coupled climate model	Online	24	2	Calculate Δ NPP by O ₃ and aerosols at 2010 and 2030
YIBs	Vegetation model	MERRA	15	S2	Evaluate O ₃ damage scheme for China PFTs
YIBs	Vegetation model	ModelE2-YIBs	30	S3	Isolate aerosol individual climatic impacts on NPP

998
999
1000
1001

^a Table index refers to the tables in [the main text and](#) supporting information.

Deleted: S2

Deleted: S3

Deleted: S4

Deleted: Page Break

Deleted: .

1007
1008
1009

Table 2. Summary of 24 online simulations with the ModelE2-YIBs model

<u>Simulations</u>	<u>Period</u>	<u>Emission Inventories</u>	<u>Emission sources</u>	<u>Ozone damage</u>	<u>Aerosol indirect effect</u>
<u>G10NATNO3</u>	<u>2010</u>	<u>GAINS^a</u>	<u>Natural</u>	<u>Null</u>	<u>No</u>
<u>G10ALLNO3</u>	<u>2010</u>	<u>GAINS</u>	<u>All^d</u>	<u>Null</u>	<u>No</u>
<u>G10ALLLO3</u>	<u>2010</u>	<u>GAINS</u>	<u>All</u>	<u>Low</u>	<u>No</u>
<u>G10ALLHO3</u>	<u>2010</u>	<u>GAINS</u>	<u>All</u>	<u>High</u>	<u>No</u>
<u>G30NATNO3</u>	<u>2030</u>	<u>GAINS CLE^b</u>	<u>Natural</u>	<u>Null</u>	<u>No</u>
<u>G30ALLNO3</u>	<u>2030</u>	<u>GAINS CLE</u>	<u>All</u>	<u>Null</u>	<u>No</u>
<u>G30ALLLO3</u>	<u>2030</u>	<u>GAINS CLE</u>	<u>All</u>	<u>Low</u>	<u>No</u>
<u>G30ALLHO3</u>	<u>2030</u>	<u>GAINS CLE</u>	<u>All</u>	<u>High</u>	<u>No</u>
<u>M30NATNO3</u>	<u>2030</u>	<u>GAINS MTFR^c</u>	<u>Natural</u>	<u>Null</u>	<u>No</u>
<u>M30ALLNO3</u>	<u>2030</u>	<u>GAINS MTFR</u>	<u>All</u>	<u>Null</u>	<u>No</u>
<u>M30ALLLO3</u>	<u>2030</u>	<u>GAINS MTFR</u>	<u>All</u>	<u>Low</u>	<u>No</u>
<u>M30ALLHO3</u>	<u>2030</u>	<u>GAINS MTFR</u>	<u>All</u>	<u>High</u>	<u>No</u>
<u>G10NATNO3_AIE</u>	<u>2010</u>	<u>GAINS</u>	<u>Natural</u>	<u>Null</u>	<u>Yes</u>
<u>G10ALLNO3_AIE</u>	<u>2010</u>	<u>GAINS</u>	<u>All</u>	<u>Null</u>	<u>Yes</u>
<u>G10ALLLO3_AIE</u>	<u>2010</u>	<u>GAINS</u>	<u>All</u>	<u>Low</u>	<u>Yes</u>
<u>G10ALLHO3_AIE</u>	<u>2010</u>	<u>GAINS</u>	<u>All</u>	<u>High</u>	<u>Yes</u>
<u>G30NATNO3_AIE</u>	<u>2030</u>	<u>GAINS CLE</u>	<u>Natural</u>	<u>Null</u>	<u>Yes</u>
<u>G30ALLNO3_AIE</u>	<u>2030</u>	<u>GAINS CLE</u>	<u>All</u>	<u>Null</u>	<u>Yes</u>
<u>G30ALLLO3_AIE</u>	<u>2030</u>	<u>GAINS CLE</u>	<u>All</u>	<u>Low</u>	<u>Yes</u>
<u>G30ALLHO3_AIE</u>	<u>2030</u>	<u>GAINS CLE</u>	<u>All</u>	<u>High</u>	<u>Yes</u>
<u>M30NATNO3_AIE</u>	<u>2030</u>	<u>GAINS MTFR</u>	<u>Natural</u>	<u>Null</u>	<u>Yes</u>
<u>M30ALLNO3_AIE</u>	<u>2030</u>	<u>GAINS MTFR</u>	<u>All</u>	<u>Null</u>	<u>Yes</u>
<u>M30ALLLO3_AIE</u>	<u>2030</u>	<u>GAINS MTFR</u>	<u>All</u>	<u>Low</u>	<u>Yes</u>
<u>M30ALLHO3_AIE</u>	<u>2030</u>	<u>GAINS MTFR</u>	<u>All</u>	<u>High</u>	<u>Yes</u>

1010 ^a GAINS is short for the v4a emission inventory of Greenhouse Gas and Air Pollution
1011 Interactions and Synergies (<http://gains.iiasa.ac.at/models/index.html>).

1012 ^b CLE is the emission scenario predicted based on current legislation emissions.

1013 ^c MTFR is the emission scenario predicted with maximum technically feasible reductions.

1014 ^d All emissions including both natural and anthropogenic sources. For the detailed
1015 anthropogenic emissions, refer to Fig. S2.

1016

1017
 1018
 1019
 1020
 1021

Table 3. Changes in NPP over China due to combined and separate effects^a of air pollution (units: Pg C yr⁻¹)

	2010	2030 CLE	2030 MFFR
O₃ (mean)^b	-0.59 ± 0.11 (-0.60 ± 0.13)	-0.67 ± 0.11 (-0.71 ± 0.16)	-0.29 ± 0.14 (-0.31 ± 0.10)
Low sensitivity	-0.43 ± 0.12 (-0.40 ± 0.13)	-0.43 ± 0.14 (-0.51 ± 0.16)	-0.22 ± 0.17 (-0.15 ± 0.10)
High sensitivity	-0.76 ± 0.15 (-0.80 ± 0.16)	-0.90 ± 0.13 (-0.92 ± 0.18)	-0.36 ± 0.16 (-0.46 ± 0.12)
Aerosol (total)^c	0.20 ± 0.08 (-0.20 ± 0.09)	0.23 ± 0.14 (-0.09 ± 0.19)	0.16 ± 0.14 (0.04 ± 0.17)
Temperature ^d	0.03 ± 0.04 (0.01 ± 0.04)	0.04 ± 0.02 (0.02 ± 0.05)	0.03 ± 0.04 (0.00 ± 0.04)
Radiation ^d	0.09 ± 0.04 (-0.03 ± 0.04)	0.16 ± 0.06 (-0.01 ± 0.06)	0.11 ± 0.04 (-0.03 ± 0.03)
Soil moisture ^d	0.07 ± 0.07 (-0.19 ± 0.10)	0.01 ± 0.09 (-0.09 ± 0.15)	0.03 ± 0.12 (0.00 ± 0.09)
O₃ + aerosol (net)^e	-0.39 ± 0.12 (-0.80 ± 0.11)	-0.43 ± 0.12 (-0.80 ± 0.10)	-0.12 ± 0.13 (-0.28 ± 0.14)

Formatted Table

1022
 1023
 1024
 1025
 1026
 1027
 1028
 1029
 1030
 1031
 1032
 1033
 1034
 1035
 1036
 1037
 1038
 1039
 1040

^a Results shown are the averages ± one standard deviation. Simulations with both aerosol direct and indirect radiative effects (AIE) are shown in the brackets.

^b Mean O₃ damages are calculated as half of differences in ΔNPP between low and high sensitivities, e.g., present-day mean O₃ damage is $\frac{1}{2}(G10ALLHO3+G10ALLLO3) - G10ALLNO3$.

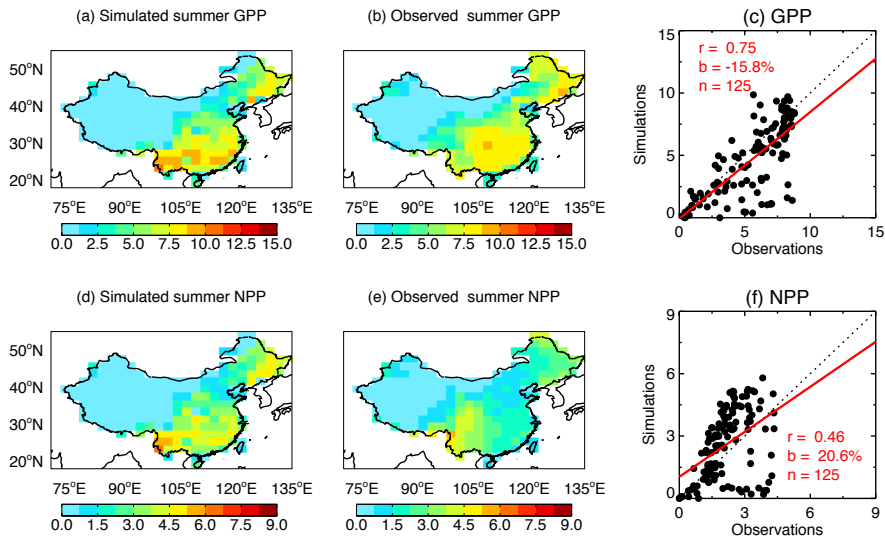
^c Combined aerosol effects are calculated with the ModelE2-YIBs climate model, e.g., present-day aerosol effect is $G10ALLNO3 - G10NATNO3$.

^d Separate aerosol effects are calculated with the offline YIBs vegetation model driven with forcings from the climate model (Table S3).

^e The net impact of O₃ damages and aerosol effects, for example at present day, is calculated as $\frac{1}{2}(G10ALLHO3+G10ALLLO3) - G10NATNO3$.

Deleted: Uncertainties for mean

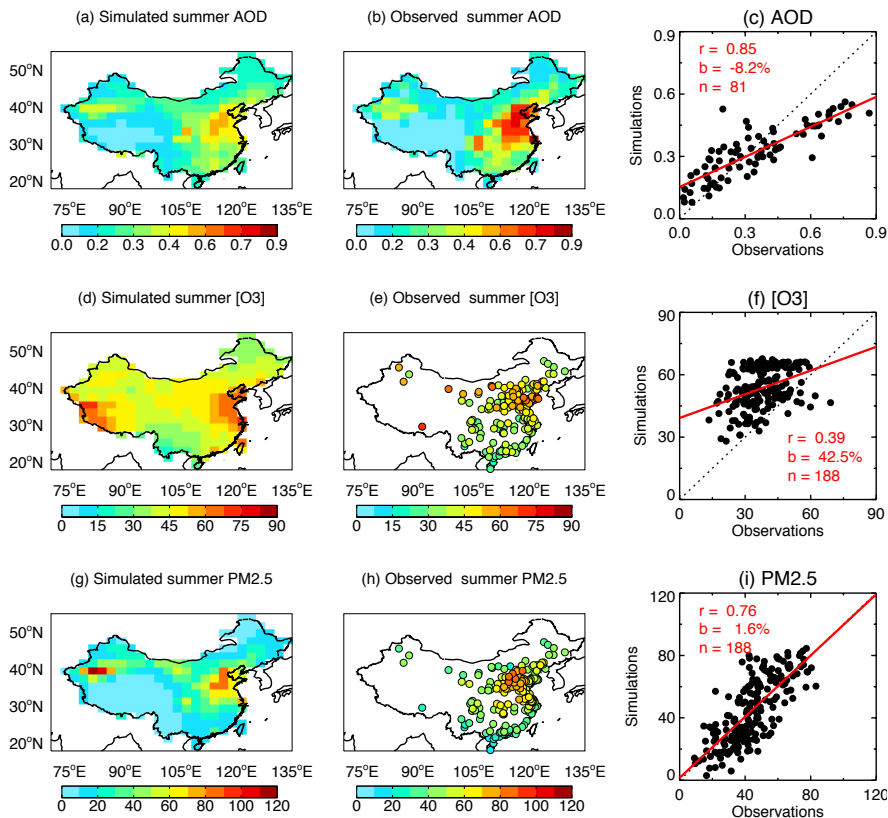
Deleted: S4



1043
 1044
 1045 **Figure 1.** Evaluation of simulated summertime carbon fluxes by ModelE2-YIBs. Panels
 1046 show GPP (top row) and NPP (bottom row) over China. Simulation results (a, d) are the
 1047 average of G10ALLHO3 and G10ALLLO3, which are performed with the climate model
 1048 ModelE2-YIBs using high and low ozone damage sensitivities (Table 2). The correlation
 1049 coefficients (r), relative biases (b), and number of grid cells (n) for the comparisons are
 1050 listed on the scatter plots. Units: $\text{g C m}^{-2} \text{ day}^{-1}$.

Deleted: S2

1051
 1052
 1053



1057
1058
1059 **Figure 2.** Evaluation of simulated summertime air pollution in China. Evaluations shown
1060 include (a) aerosol optical depth (AOD) at 550 nm, (d) [O₃] (units: ppbv), and (g) PM_{2.5}
1061 concentrations (units: $\mu\text{g m}^{-3}$) with observations from (b) the satellite retrieval of the
1062 MODIS (averaged for 2008-2012), and (e) and (h) measurements from 188 ground-based
1063 sites (at the year 2014). Simulation results are from G10ALLNO3 performed with the
1064 climate model ModelE2-YIBs (Table 2). The correlation coefficients (r), relative biases
1065 (b), and number of sites/grids (n) for the comparisons are listed on the scatter plots.

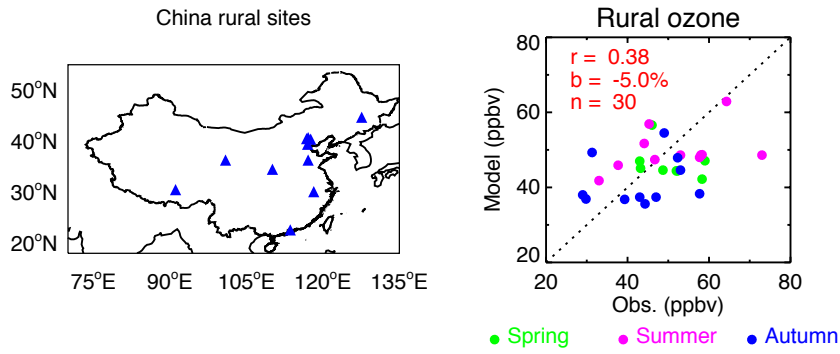
Formatted: Subscript

Deleted: ,

Deleted: .

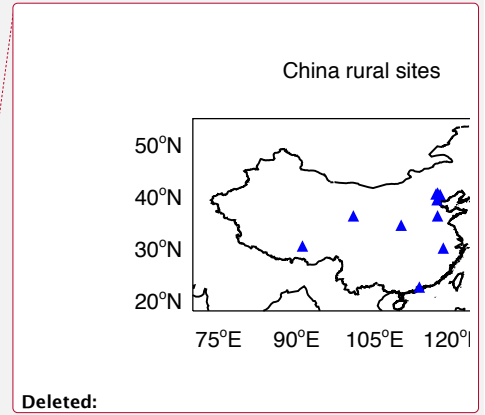
Deleted: S2

1071
1072



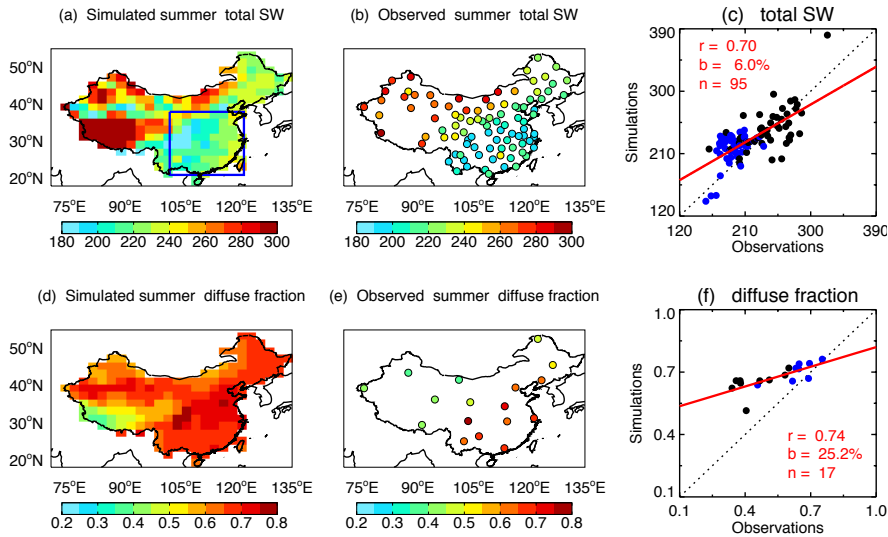
1073
1074 **Figure 3.** Evaluation of simulated [O₃] at rural sites in China. Simulation results are from
1075 G10ALLNO3 performed with the climate model ModelE2-YIBs (Table 2). For the scatter
1076 plots, green, pink, and blue points represent values in spring, summer, and autumn,
1077 respectively. The data sources of all sites are listed in Table S4.

1078
1079



- Deleted: NASA
- Deleted: S2
- Deleted: S5

1084
1085
1086

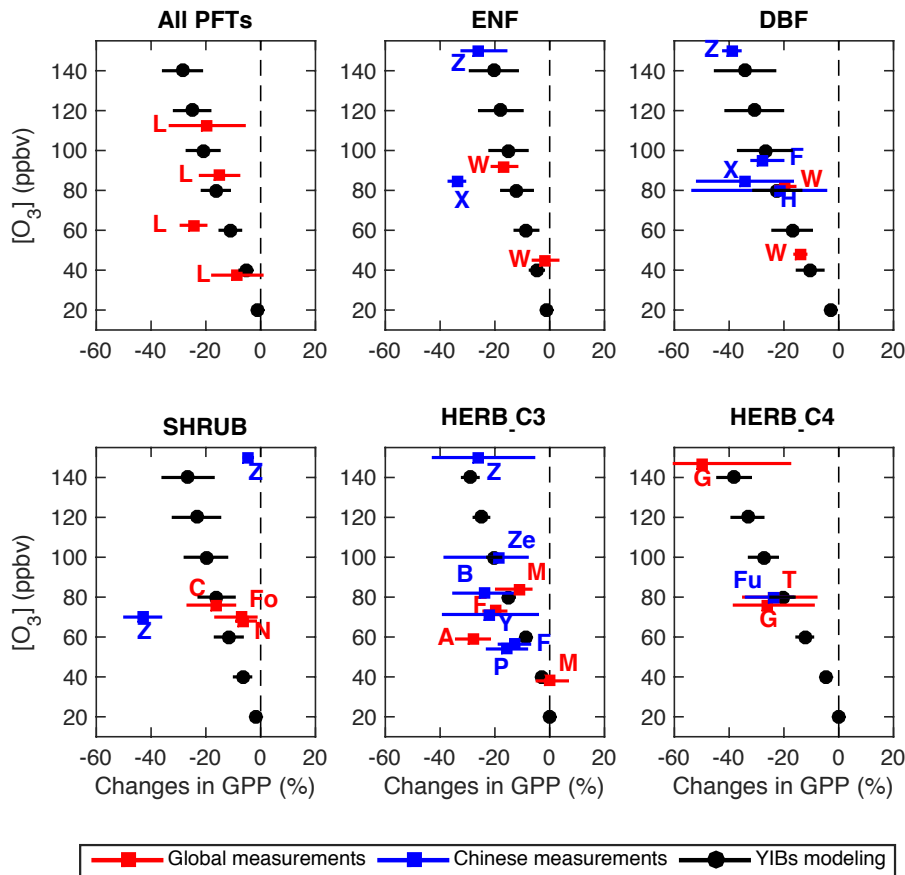


1087
1088
1089
1090
1091
1092
1093
1094
1095
1096

Figure 4. Evaluation of simulated radiation fluxes by ModelE2-YIBs. Panels show summertime surface (a) total shortwave radiation (units: W m^{-2}) and (d) diffuse-to-total fraction with (b, e) observations from 106 sites. Simulation results are from G10ALLNO3 performed with the climate model ModelE2-YIBs (Table 2). The correlation coefficients (r), relative biases (b), and number of sites (n) for the comparisons are listed on the (c, f) scatter plots. The blue points in the scatter plots represent sites located within the box regions in southeastern China as shown in (a).

Deleted: NASA

Deleted: S2



1099
 1100 **Figure 5.** Comparison of predicted changes in summer GPP by O₃ with measurements.
 1101 Simulations are performed using the offline YIBs vegetation model (Table S2) and
 1102 averaged for all grid squares over China weighted by the area of a specific PFT. Black
 1103 points show the simulated mean reductions with error bars indicating damage range from
 1104 low to high O₃ sensitivity. Solid squares with error bars show the results (mean plus
 1105 uncertainty) based on measurements reported in the literature (Table S1). Experiments
 1106 performed for vegetation types in China are denoted with blue symbols. The author initials
 1107 are indicated for the corresponding studies.

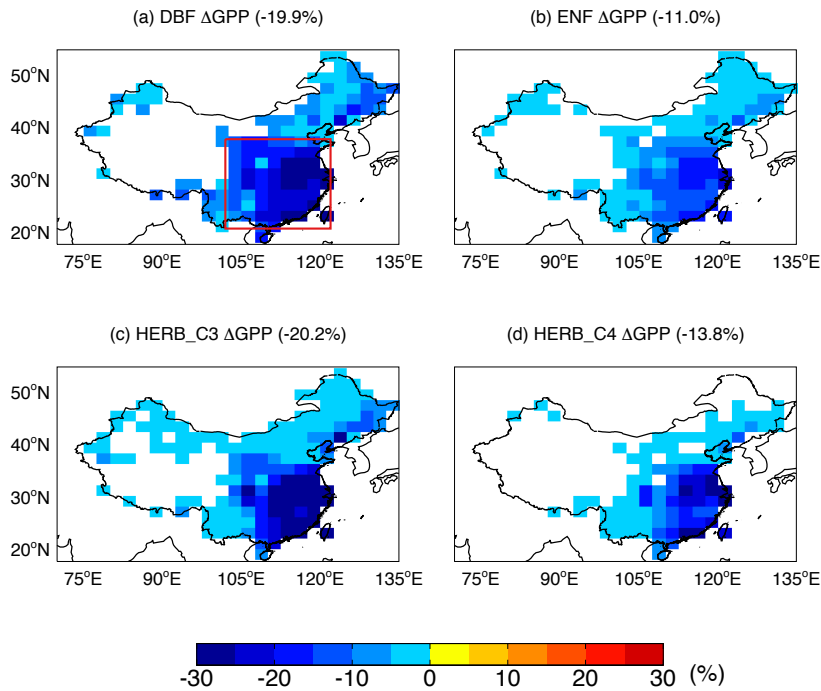
Formatted: Justified, Line spacing: 1.5 lines

Deleted: S3

Deleted: .

Formatted: Font:Bold

1110
1111

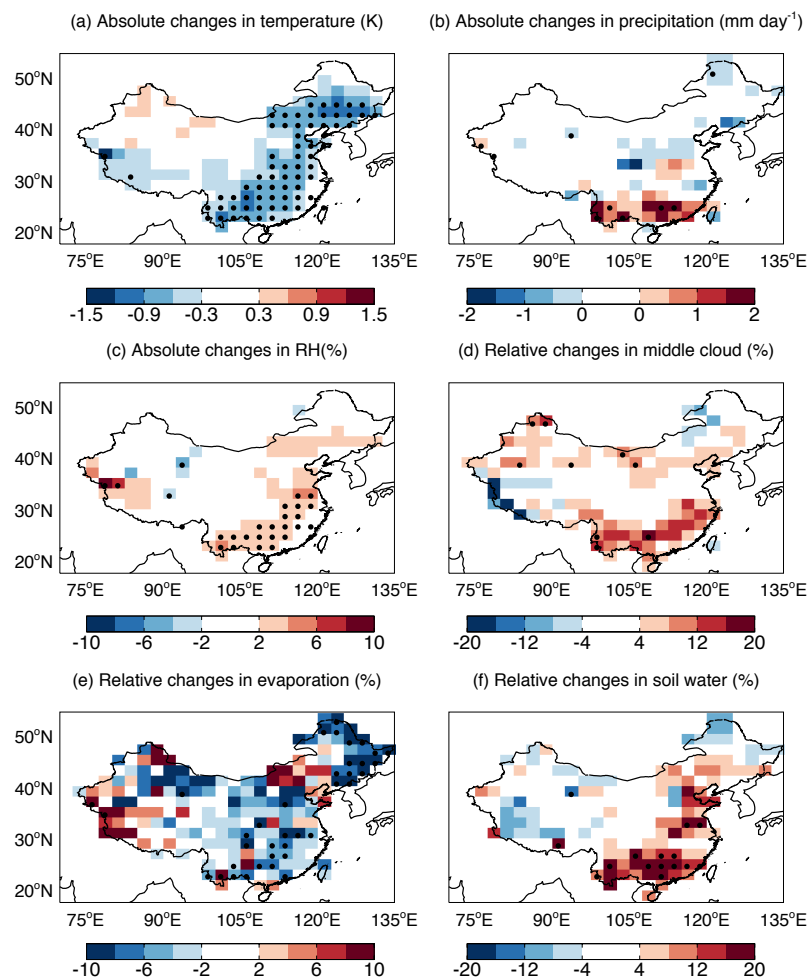


1112
1113
1114 **Figure 6.** Predicted offline percentage damage to summer GPP caused by O₃. Panels show
1115 the damages to (a) ENF (evergreen needleleaf forest), (b) DBF (deciduous broadleaf
1116 forest), (c) C3 herbs, and (d) C4 herbs over China in the year 2010. Simulations are
1117 performed with the climate model ModelE2-YIBs, which does not feed O₃ vegetation
1118 damages back to affect biometeorology, plant growth, and ecosystem physiology. The
1119 results are averaged for the low and high damaging sensitivities:

$$1120 \quad \left(\frac{1}{2}(G10ALLHO3_OFF+G10ALLLO3_OFF)/G10ALLNO3 - 1\right) \times 100\%$$

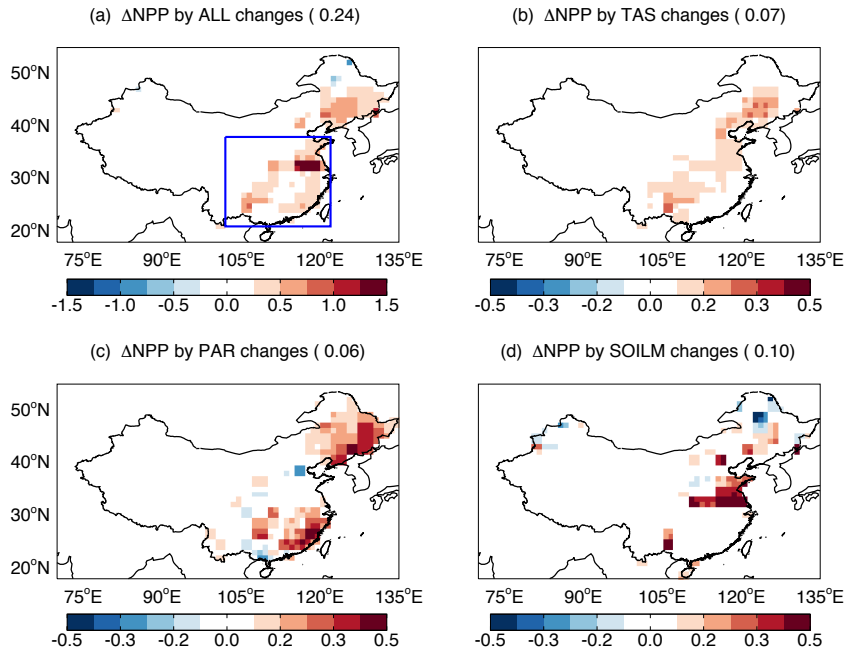
1121 The average value over the box domain of (a) is shown in the title bracket of each subpanel.

1122
1123



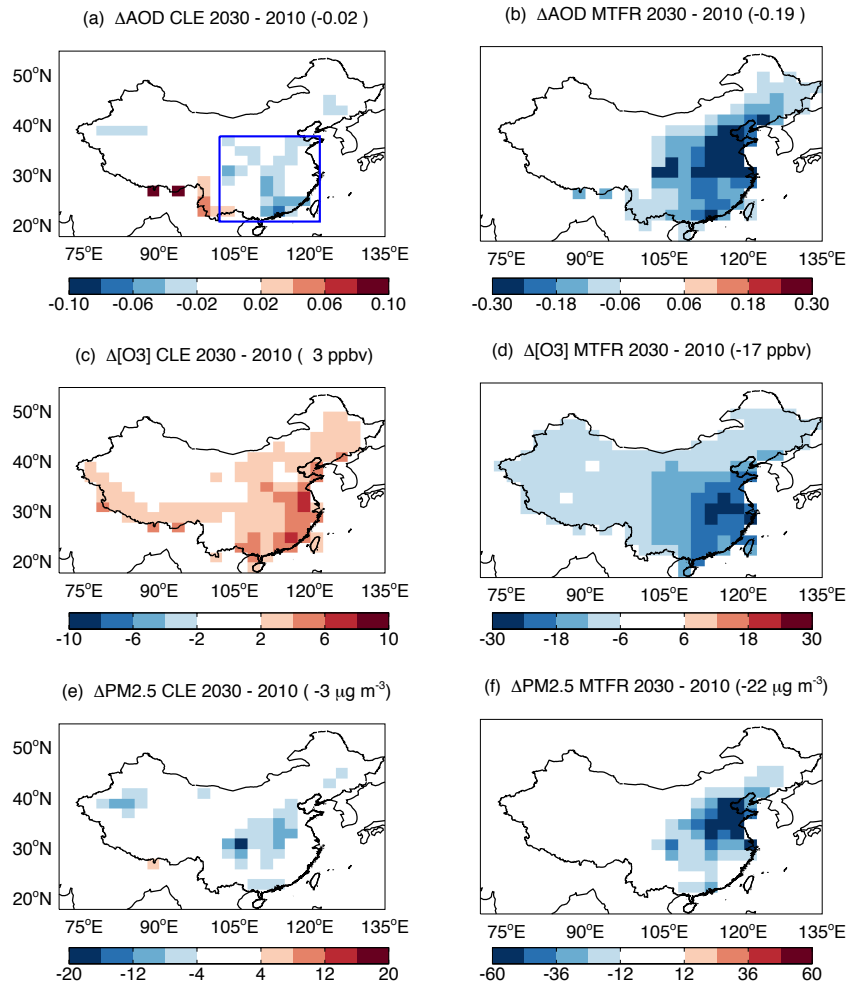
1124
 1125
 1126 **Figure 7.** Changes in summer meteorology due to direct radiative effects of anthropogenic
 1127 aerosols. All changes are calculated as the differences between the simulations
 1128 G10ALLNO3 and G10NATNO3. For (a) temperature, (b) precipitation, and (c) relative
 1129 humidity, we show the absolute changes as $G10ALLNO3 - G10NATNO3$. For (d) middle
 1130 cloud cover, (e) evaporation, and (f) soil water content, we show the relative changes as
 1131 $(G10ALLNO3/G10NATNO3 - 1) \times 100\%$. Significant changes ($p < 0.05$) are marked with
 1132 black dots.
 1133

1134
1135
1136



1137
1138
1139 **Figure 8.** Decomposition of aerosol-induced changes in summer NPP. Changes in NPP are
1140 caused by aerosol-induced changes in (b) surface air temperature, (c) photosynthetically
1141 active radiation (PAR), (d) soil moisture, and (a) the combination of above three effects.
1142 Simulations are performed with the offline YIBs vegetation model driven with
1143 meteorological forcings simulated with the ModelE2-YIBs climate model (Table S3). The
1144 NPP responses to PAR include the DRF effects. The color scale for the first panel is
1145 different from the others. The average NPP perturbation over the box domain in a is shown
1146 in the bracket of each title. Units: $\text{g C m}^{-2} \text{ day}^{-1}$.
1147
1148

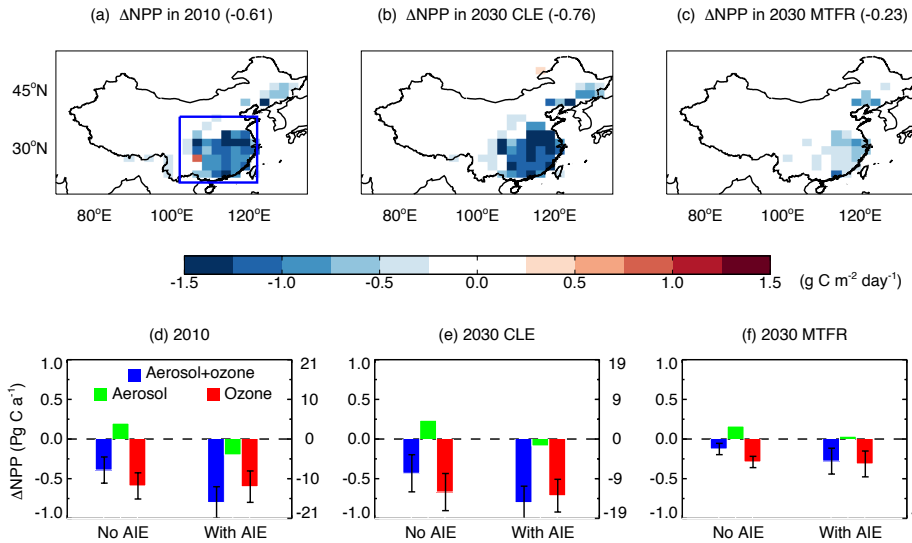
Deleted: S4).



1150
 1151 **Figure 9.** Predicted changes in summertime air pollution by 2030. Panels shown are for (a,
 1152 b) AOD, (c, d) $[\text{O}_3]$, and (e, f) $\text{PM}_{2.5}$ concentrations for the year 2030 relative to 2010 based
 1153 on scenarios of (left) current legislation emissions (CLE) and (right) maximum technically
 1154 feasible reduction (MTRF). Results for the left panels are calculated as (G30ALLNO3 –
 1155 G10ALLNO3). Results for the right panels are calculated as (M30ALLNO3 –
 1156 G10ALLNO3). The average value over the box domain of (a) is shown in the title bracket
 1157 of each subpanel.
 1158

Formatted: Subscript

1159
1160



1161
1162

1163 **Figure 10.** Impacts of air pollution on NPP in the whole of China. Results shown are
1164 combined effects of aerosol and O_3 on the summer NPP in (a) 2010, (b) 2030 with CLE
1165 scenario, and (c) 2030 with MTRF scenario. Results for the top panels do not include
1166 aerosol indirect effects (AIE) but do include the meteorological response to aerosol direct
1167 radiative effects. The average NPP perturbation over the box domain in (a) is shown in the
1168 bracket of each title. The perturbations to annual total NPP by aerosol, O_3 , and their sum
1169 over the whole China are shown in (d-f) for different periods, with (right) and without (left)
1170 inclusion of AIE. Damages by O_3 are averaged for low and high sensitivities with error
1171 bars indicating ranges. The percentage changes are calculated based on NPP without AIE.
1172 Simulations are performed with the ModelE2-YIBs model. Only the significant changes (p
1173 < 0.05) are shown in (a-c).

1174
1175